VTT PUBLICATIONS 367

Master curve analysis of ductile to brittle transition region fracture toughness round robin data

The "EURO" fracture toughness curve

Kim Wallin

VTT Manufacturing Technology

TECHNICAL RESEARCH CENTRE OF FINLAND
ESPOO 1998

ISBN 951–38–5345–4 (soft back ed.)
ISSN 1235–0621 (soft back ed.)

ISBN 951–38–5346–2 (URL: http://www.inf.vtt.fi/pdf/)
ISSN 1455–0849 (URL: http://www.inf.vtt.fi/pdf/)

JULKAISIJA – UTGIVARE – PUBLISHER

Valtion teknillinen tutkimuskeskus (VTT), Vuorimiehentie 5, PL 2000, 02044 VTT
puh. vaihde (09) 4561, faksi (09) 456 4374

Statens tekniska forskningscentral (VTT), Bergsmansvägen 5, PB 2000, 02044 VTT
tel. växel (09) 4561, fax (09) 456 4374

Technical Research Centre of Finland (VTT), Vuorimiehentie 5, P.O.Box 2000, FIN–02044 VTT, Finland
phone internat. + 358 9 4561, fax + 358 9 456 4374

VTT Valmistustekniikka, Voimalaitosten materiaalitekniikka, Kemistintie 3, PL 1704, 02044 VTT
puh. vaihde (09) 4561, faksi (09) 456 7002

VTT Tillverkningsteknik, Material och strukturell integritet, Kemistvägen 3, PB 1704, 02044 VTT
tel. växel (09) 4561, fax (09) 456 7002

VTT Manufacturing Technology, Materials and Structural Integrity, Kemistintie 3, P.O.Box 1704, FIN–02044 VTT, Finland
phone international +358 9 4561, fax +358 9 456 7002

Technical editing Leena Ukskoski

Libella Painopalvelu Oy, Espoo 1998

Wallin, Kim. Master curve analysis of ductile to brittle transition region fracture toughness round robin data. The "EURO" fracture toughness curve. Espoo 1998, Technical Research Centre of Finland, VTT Publications 367. 58 p.

Keywords fractures (materials), steels, fracture strength, ductile brittle transition, brittleness, statistical analysis, master curve method

Abstract

Brittle fracture in the ductile to brittle transition regime is connected with specimen size effects and - more importantly- tremendous scatter of fracture toughness, which the technical community is currently becoming increasingly aware of. The size effects have the consequence that fracture toughness data obtained from small laboratory specimens do not directly describe the fracture behaviour of real flawed structures. Intensive research has been conducted in the last decade in order to overcome these problems. Different approaches have been developed and proposed, one of the most promising being the master curve method, developed at VTT Manufacturing Technology.

For validation purposes, a large nuclear grade pressure vessel forging 22NiMoCr37 (A508 Cl.2) has been extensively characterised with fracture toughness testing. The tests have been performed on standard geometry CT-specimens having thickness 12.5 mm, 25 mm, 50 mm and 100 mm. The a/W-ratio is close to 0.6 for all specimens. One set of specimens had 20% side-grooves. The obtained data consists of a total of 757 results fulfilling the ESIS-P2 test method validity requirements with respect to pre-fatigue crack shape and the ASTM E-1921 pre-fatigue load. The master curve statistical analysis method is meticuously applied on the data, in order to verify the validity of the method. Based on the analysis it can be concluded that the validity of all the assumptions in the master curve method is confirmed for this material.

Preface

This work is part of the Measurements and Testing Programme of the European Community Project: "Fracture Toughness of Steel in the Ductile to Brittle Transition Regime" Contract No. MAT-CT-940080, co-ordinated by GKSS-Forschungszentrum Geesthacht. The VTT participation in the project is part of the national Material Degradation in Reactor Environment project (RAVA) belonging to the Structural Integrity of NPP's research programme (RATU2), performed at VTT Manufacturing Technology and financed by the Ministry of Trade and Industry in Finland (KTM), Technical Research Centre of Finland (VTT), Radiation and Nuclear Safety Authority (STUK), and Finnish nuclear power industry.

Contents

1. Introduction

The European Structural Integrity Society (ESIS) and the International Standardisation Organisation (ISO) are currently drafting test standards for characterising the fracture toughness of metals which are supposed to be basis for CEN standards. The drafts include also the characterisation of the transition from ductile to brittle fracture of steels.

However, this transition region is connected with specimen size effects and – more importantly – tremendous scatter of fracture toughness, which the technical community is currently becoming increasingly aware of.

The size effects have the consequence that fracture toughness data obtained from small laboratory specimens do not directly describe the fracture behaviour of real flawed structures. Intensive research has been conducted in the last decade in order to overcome these problems. Different approaches have been developed and proposed, one of the most promising being the master curve method, developed at VTT Manufacturing Technology. The master curve method, provides a description for the fracture toughness scatter, size effect and temperature dependence both for the transition region as well as the lower shelf. The master curve method has already led to an American testing and analysis standard ASTM E1921-98 and it is an obvious candidate for European standardisation. In order to verify the validity of the master curve method and other proposed methods, a sufficiently large data set which shows continuously the scatter and the size effects from the lower shelf to the upper shelf of a single material is needed. Such a data has not existed until now.

In 1995 a project entitled "Fracture Toughness of Steel in the Ductile to Brittle Transition Regime" was launched under the "Measurement and Testing Programme of the European Community". In the project, more than 750, specimens of four different sizes have been tested at different temperatures to produce a sufficiently large data set for the validation of the different statistical methods. In this report, the data from the project is meticulously analysed with the, VTT based, master curve method and the validity of the different aspects of the method is verified, both separately and in combination.

2. Analysis method

2.1 Master curve distribution

The master curve cumulative failure probability distribution has the form (Eq. 1) [1].

$$P_f = 1 - \exp\left\{-\left(\frac{K_{JC} - K_{\min}}{K_0 - K_{\min}}\right)^4\right\} \quad (1)$$

2.2 Failure probability diagram

The single temperature data is presented in the "original" master curve failure probability diagram which produces a linear presentation of the master curve cumulative failure probability distribution (Eq. 2, Fig. 1) [1].

$$\left\{\ln\frac{1}{1-P_f}\right\}^{1/4} = \frac{K_{Jc} - K_{\min}}{K_0 - K_{\min}} \quad (2)$$

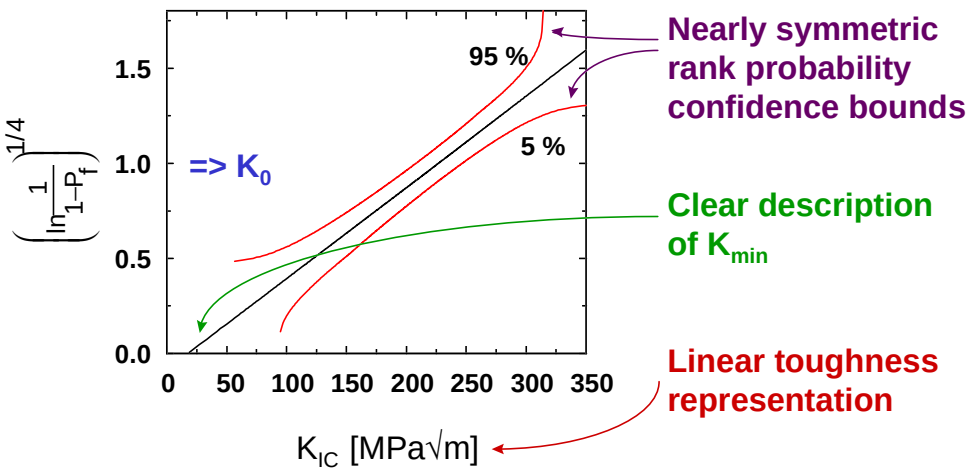

Figure 1. Master curve failure probability diagram.

Compared to a normal Weibull probability diagram, the master curve failure probability diagram offers a better visualisation of the data with respect to the master curve distribution, as indicated in Fig. 1.

2.3 Rank probability

When the data is plotted into the failure probability diagram, it must be ordered by rank and designated rank probabilities. The weakness with the rank probability estimates are that they are not measured values, but estimates of cumulative probability based on order statistics. Each data point corresponds to a certain cumulative failure probability with a certain confidence. This can be expressed in a mathematical form, using the binomial distribution, as [2]

$$z' = 1 - \sum_{j=1}^{i} \frac{n!}{(j-1)! \cdot (n-j+1)!} \cdot P_{rank}^{j-1} \cdot (1 - P_{rank})^{n-j+1} \qquad (3)$$

where z' is the probability that the rank estimate corresponds to the cumulative probability P_{rank}, n is the number of points and i is the rank number. Eq. 3 can be used to calculate rank confidence estimates like the ones presented in Fig. 1. Usually people prefer to use simple approximations of the median rank probability estimate (z' = 0.5). Three common estimates of the median rank probability are [2]

$$P_{rank} = \frac{i - 0.5}{n} \qquad (4a)$$

$$P_{rank} = \frac{i}{n+1} \qquad (4b)$$

$$P_{rank} = \frac{i - 0.3}{n + 0.4} \qquad (4c)$$

The three approximations are compared with the outcome of Eq. 3 in Fig. 2. It can be seen that Eq. 4c is clearly the best estimate of the median rank probability. Thus, Eq. 4c is used for the presentation of the single temperature round robin data.

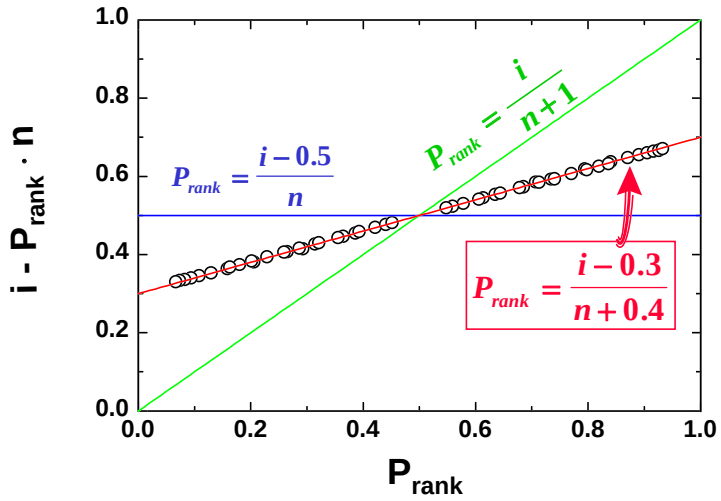

Figure 2. Comparison of different estimates of median rank probability (lines) with binomial theory estimate (circles).

2.4 K_0 estimation

The estimation of the normalisation toughness K_0 (corresponding to 63.2% failure probability) is based on the randomly censored Maximum Likelihood expression (Eq. 5) [3].

$$K_0 = \left(\frac{\sum_{i=1}^{n} \left(K_i - K_{\min}\right)^4}{\sum_{i=1}^{n} \delta_i - 1 + \ln 2} \right)^{1/4} + K_{\min} \qquad (5)$$

where the censoring parameter δ_i is 1 for uncensored and 0 for censored data and the limiting fracture toughness K_{min} is fixed as 20 MPa√m.

The accuracy of the K_0 estimate will be a function of uncensored data $r = \sum_{i=1}^{n} \delta_i$.

The standard deviation of the bias corrected MML estimate is approximately [3]

$$\sigma_{\hat{K}_0 - K_{\min}} \approx \frac{0.28 \cdot (K_0 - K_{\min})}{\sqrt{r}} \tag{6}$$

An important feature, of the MML estimate, to note is that, the accuracy of the K_0 is not affected by the degree of censoring, i.e. it is not affected by the n/r ratio. Nor is it affected by the nature of censoring (random, upper end, lower end, etc.) It is only a function of the number of uncensored data (r). This can easily be verified by e.g. Monte Carlo simulations, using different censoring criteria and degrees of censoring. This property makes the MML procedure extremely valuable. In principle, not a single test result (fulfilling the requirements related to fatigue precracking, crack shape and test performance) needs to be omitted from the analysis. Any invalid data can be given the toughness value corresponding to the validity criteria and be treated as non-failures.

2.5 Censoring

Two levels of censoring are applied. First, all data referring to “non-cleavage” (ductile end of test) are prescribed $\delta_i = 0$. Second, all data violating the specimen size validity criterion (Eq. 7) were designated the toughness value corresponding to the validity criteria and given $\delta_i = 0$.

The specimen size validity criterion (taken same as in the ASTM master curve standard [4]) has the form

$$K_{JC} \le \sqrt{\frac{b \cdot \sigma_y \cdot E}{M \cdot \left(1 - \upsilon^2\right)}} \tag{7}$$

where σ_y is yield strength, E is the modulus of elasticity, the controlling dimension is the ligament size b and the size criterion constant **M = 30**.

2.6 Thickness adjustment

For the comparison of different size specimen data and for the calculation of the master curve transition temperature T_0 all data is thickness adjusted to the reference flaw length (thickness) B_0 = 25 mm with Eq. 8 [5].

$$K_{25mm} = K_{\min} + (K_{JC} - K_{\min}) \cdot \left(\frac{B}{B_0} \right)^{1/4} \tag{8}$$

The thickness B refers to the nominal thickness, regardless of side-grooving. I.e. *the 25 mm thick side-grooved specimens tested at -20°C, having a net thickness of 20 mm, are treated as being 25 mm thick.*

2.7 Temperature dependence

In the master curve concept, a constant temperature dependence for cleavage fracture toughness is assumed (Eq. 9) [6, 7].

$$K_0 = 31 + 77 \cdot \exp\left\{0.019 \cdot (T - T_0)\right\} \tag{9}$$

The transition temperature T_0 corresponds to the temperature where the mean (median) fracture toughness for a 25 mm thick specimen has the value 100 MPa√m.

2.8 T_0 estimation

Two methods of estimating the master curve transition temperature T_0 are used. First, for the single temperature data, T_0 is calculated from the size adjusted K_0 values using Eq. 9. Second, for the multi-temperature data, T_0 is estimated from the size adjusted K_{Jc} data using a multi-temperature randomly censored maximum likelihood expression (Eq. 10) [8].

$$\sum_{i=1}^{n} \frac{\delta_i \cdot \exp\left\{0.019 \cdot \left[T_i - T_0\right]\right\}}{11 + 77 \cdot \exp\left\{0.019 \cdot \left[T_i - T_0\right]\right\}} - \sum_{i=1}^{n} \frac{\left(K_{IC_i} - 20\right)^4 \cdot \exp\left\{0.019 \cdot \left[T_i - T_0\right]\right\}}{\left(11 + 77 \cdot \exp\left\{0.019\left[T_i - T_0\right]\right\}\right)^5} = 0 \qquad (10)$$

The transition temperature T_0 is solved iteratively from Eq. 10.

Since the accuracy of the K_0 estimate is proportionally constant with respect to K_0 (Eq. 6), the accuracy of the T_0 will be a function of K_0. Low K_0 leads to large uncertainty in T_0 and high K_0 leads to small uncertainty in T_0 (Fig. 3).

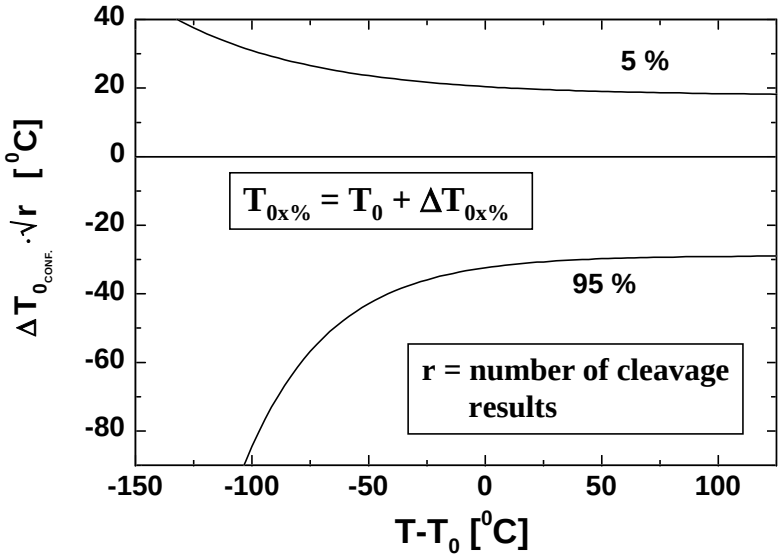

Figure 3. 5% and 95% confidence bounds for MML T_0 estimate.

2.9 K_{min} estimation

In addition to the standard maximum likelihood expression (using a fixed value of K_{min} [20 MPa√m]), also the more complicated procedure of fitting both K_0 and K_{min} was applied. The randomly censored maximum likelihood expression for fitting both K_0 and K_{min} is (Eq. 11) [2]

$$\frac{3}{4}\cdot\frac{\sum_{i=1}^{n}\frac{\delta_i}{K_i-\hat{K}_{\min}}\cdot\sum_{i=1}^{n}\left(K_i-\hat{K}_{\min}\right)^4}{\sum_{i=1}^{n}\delta_i\cdot\sum_{i=1}^{n}\left(K_i-\hat{K}_{\min}\right)^3}-1=0\Rightarrow \textit{estimate of}\ \hat{K}_{\min}$$

$$K_0=\left(\frac{\sum_{i=1}^{n}\left(K_i-\hat{K}_{\min}\right)^4}{\sum_{i=1}^{n}\delta_i-1+\ln 2}\right)^{1/4}+\hat{K}_{\min} \qquad (11)$$

$$K_{\min}=\frac{\sum_{i=1}^{n}\delta_i\cdot\hat{K}_{\min}-K_0}{\sum_{i=1}^{n}\delta_i-1}$$

where the censoring parameter δ_i is 1 for uncensored and 0 for censored data. Eq. 11 includes a small bias correction for both K_0 and K_{min}.

The accuracy of the K_{min} estimate is a function of number of uncensored data and the ratio between K_0/K_{min} (Fig. 4) [9].

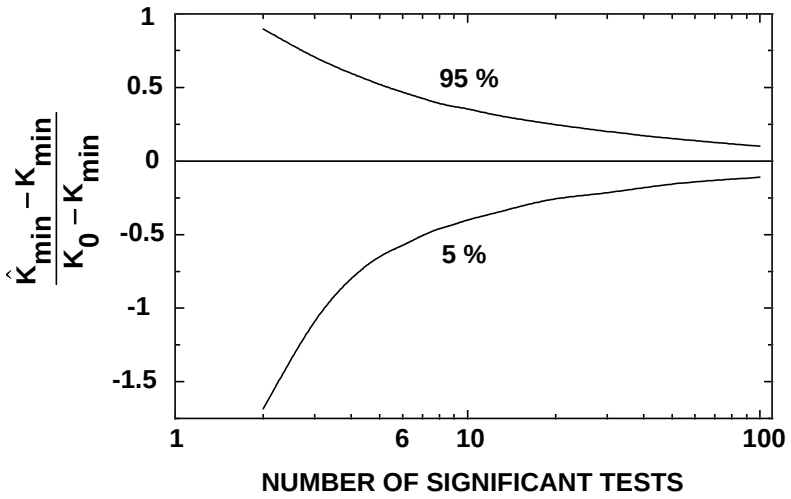

Figure 4. Accuracy of $\hat{K}_{\min}$ *MML estimate.*

2.10 Lower shelf analysis

The above derivations are based on the assumption that the probability of cleavage initiation is less than unity. This is normal for configurations like plain and notched specimens and cracked specimens in cases where initiation is sufficiently difficult. For material conditions where initiation is simple, the probability of cleavage initiation in the case of a crack may become unity. This can occur on the so called “lower shelf” of the material. Essentially it means that all possible initiation sites are activated and initiation occurs as soon as the crack is loaded, making the initiation event independent of the load level (and subsequently independent of specimen thickness). Thus, in the case of a crack, the lower shelf toughness may be controlled purely by the probability of propagation. For plain and notched configurations, however, the probability of initiation will still be a function of load level even on the lower shelf. Therefore, a simple correlation between notched and cracked configurations may not be possible for the lower shelf material conditions.

The three data sets corresponding to test temperature -154^{0}C, are additionally analysed with a special equation developed for the propagation controlled lower shelf behaviour of fracture toughness.

The equation has the form (Eq. 12) [10]

$$P_{f4LS} = 1 - \exp\left\{ - \frac{K_{min4}}{K_{e4}} \cdot \left[\frac{K_I}{K_{min4}} - 3 \cdot \ln\left(\frac{K_I}{K_{min4}} \right) - 3 \cdot \frac{K_{min4}}{K_1} + \frac{1}{2}\left(\frac{K_{min4}}{K_I} \right)^2 + \frac{3}{2} \right] \right\} \quad (12)$$

where K_{min4} is the lower shelf limiting minimum fracture toughness and K_{e4} is a normalisation fracture toughness.

The biggest difference between the lower shelf expression and the transition region expression is that the lower shelf expression does not predict a statistical size effect.

3. Preliminary analysis

3.1 Material

All specimens were extracted from a single segment of a large nuclear grade pressure vessel forging 22NiMoCr37 (A508 Cl.2) so that the crack front was located in the region ¼T–½T which had been found to be "homogeneous" in the preliminary investigations performed by GKSS [11]. The sectioning diagram is presented in Fig. 5.

Due to available time and resources, the specimens were not randomly distributed throughout the forging, but instead the large segment was divided into smaller sections from which different size specimens were manufactured and tested at one temperature. All the larger specimens could not be extracted form the same section as the small specimens, but an effort was made to take them comparatively close from the small specimen sections.

3.2 Test details

The fracture toughness tests were performed on standard geometry CT-specimens having thickness 12.5 mm, 25 mm, 50 mm and 100 mm. The a/W-ratio was close to 0.6 for all specimens.

The fracture toughness tests were performed essentially in accordance with the ESIS P2 procedure without performing a crack growth correction on the J-integral. The main deviation from the ESIS P2 procedure occurred for the pre-fatigue of the specimens, which was performed in line with the ASTM E-1921 standard. One set of 25 mm thick specimens tested at -20^{o}C was side-grooved 20% (10% + 10%). All specimens were loaded either until occurrence of brittle fracture or until the load drop due to ductile tearing equalled 20% of the maximum load.

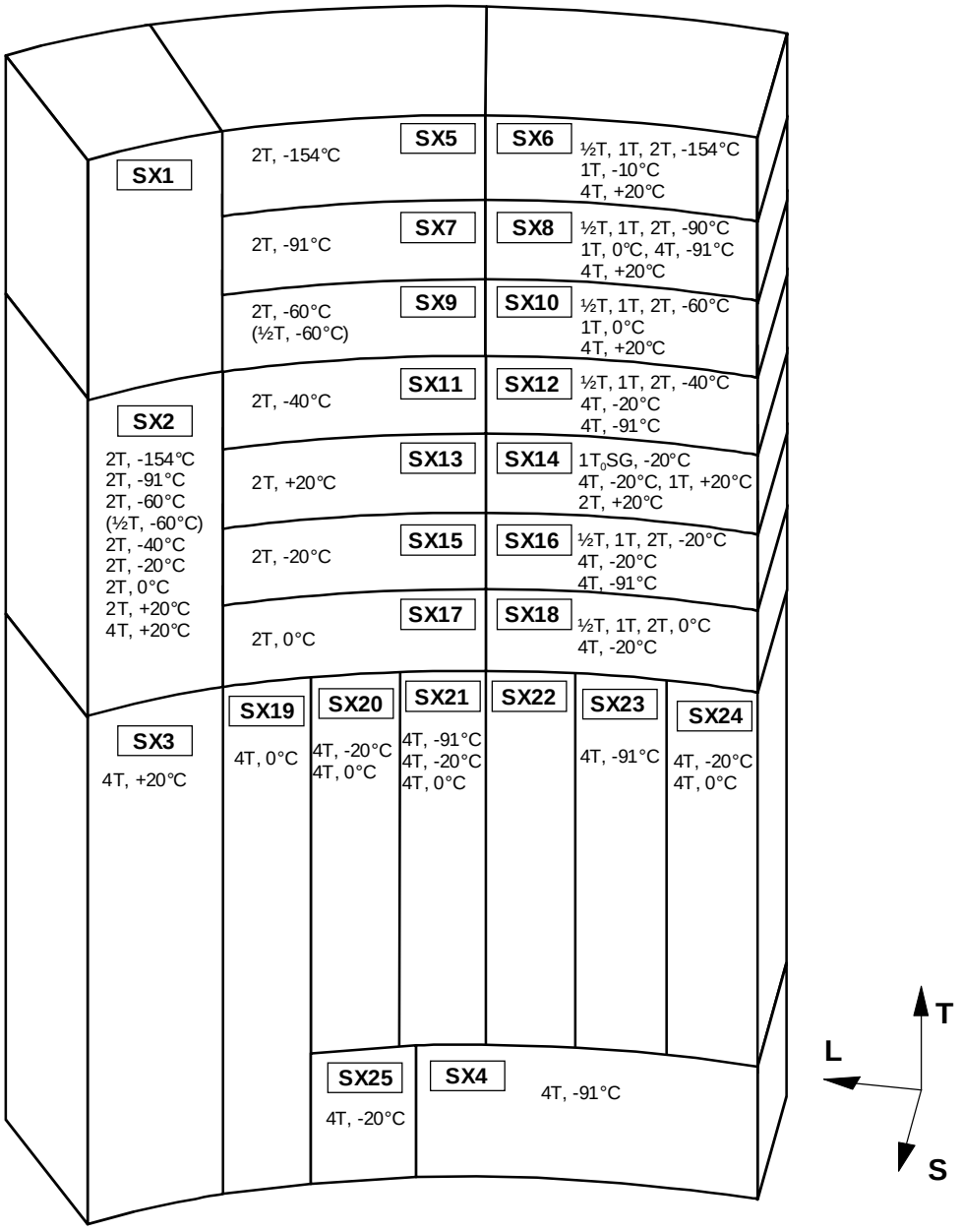

Figure 5. Sectioning diagram of 22NiMoCr37.

The measured J-integral values were transformed into K_{Jc} values with the equation

$$K_{JC} = \sqrt{\frac{J \cdot 206\,GPa}{0.91}} \qquad (13)$$

i.e. a constant modulus of elasticity and plane strain conditions were assumed for all temperatures.

A more detailed description of the project background and test performance is presented elsewhere [11].

3.3 Yield stress

The measured yield stress values were fitted by an exponential temperature dependence expression, the result of which is presented in Fig. 6.

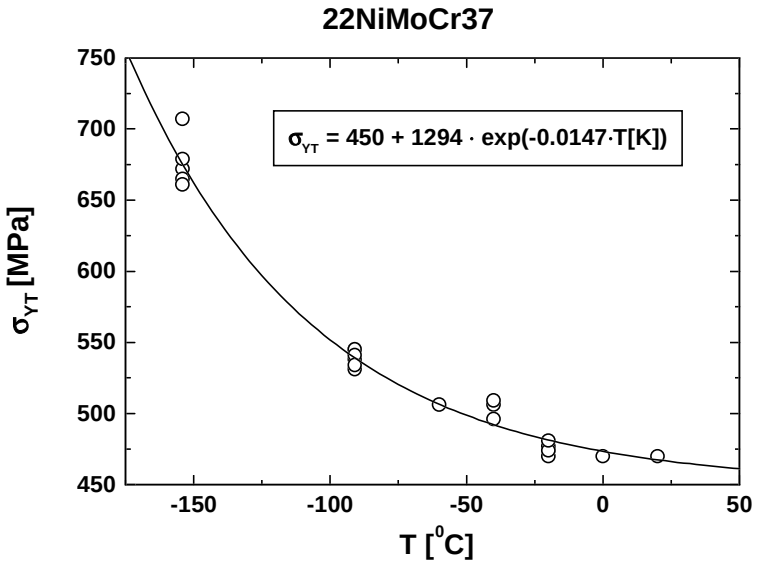

Figure 6. Yield stress temperature dependence.

3.4 Raw data

All the fracture toughness results, fulfilling the initial crack front straightness and pre-fatigue criteria, are presented in Fig. 7. The data is unadjusted "raw" data. In addition to the fracture toughness, also the amount of ductile tearing preceding brittle fracture was measured optically. The resulting multi-specimen K_{Jc}-Δa-curve is presented in Fig. 8. In Fig. 8, all specimens failing by cleavage have been included. Thus also data referring to values beyond maximum load are included. Only beyond the values shown in Fig. 8 the K_{Jc}-Δa-curves start to show a clear size dependence (small specimens yield lower curves).

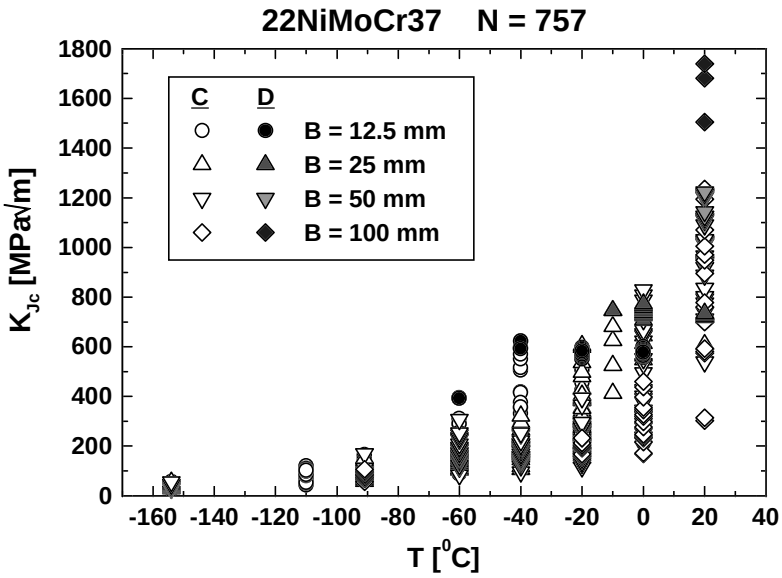

Figure 7. "Raw" fracture toughness data. Filled points refer to ductile end of test values.

The K_J values corresponding to ductile load maximum are presented in Fig. 9. A remarkable resemblance between Figs 8 and 9 is clear. The two plots seem to represent the same tearing resistance curve. This indicates that the amount of crack growth at maximum load is directly proportional to the specimen ligament size (not thickness of specimen) and the maximum load value corresponds only to a specific location on the tearing resistance curve. The amount of ductile tearing at maximum load will also be a function of the materials tearing resistance and strain hardening, but for a single material and specimen type, the controlling parameter will be the ligament size. This result gives a clear interpretation of the relevance of the ductile maximum load fracture toughness.

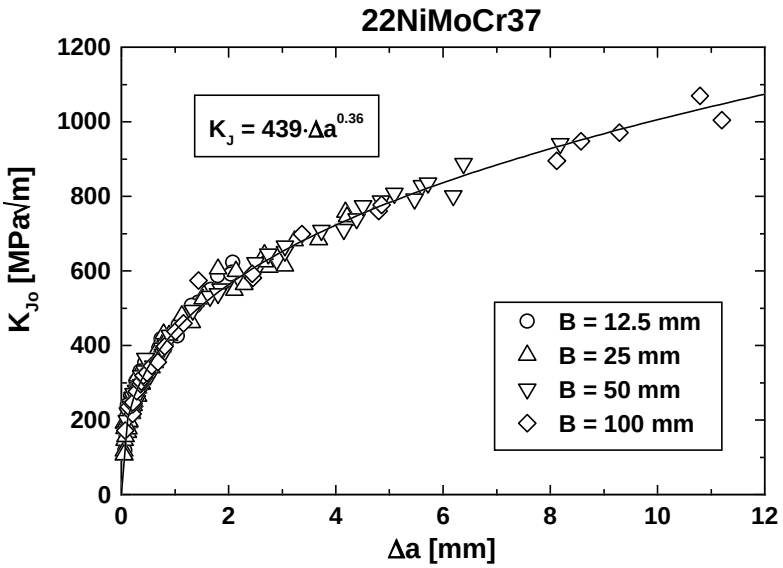

Figure 8. Multi-specimen (cleavage fracture) K_J-Δa-curve showing no effect of specimen size.

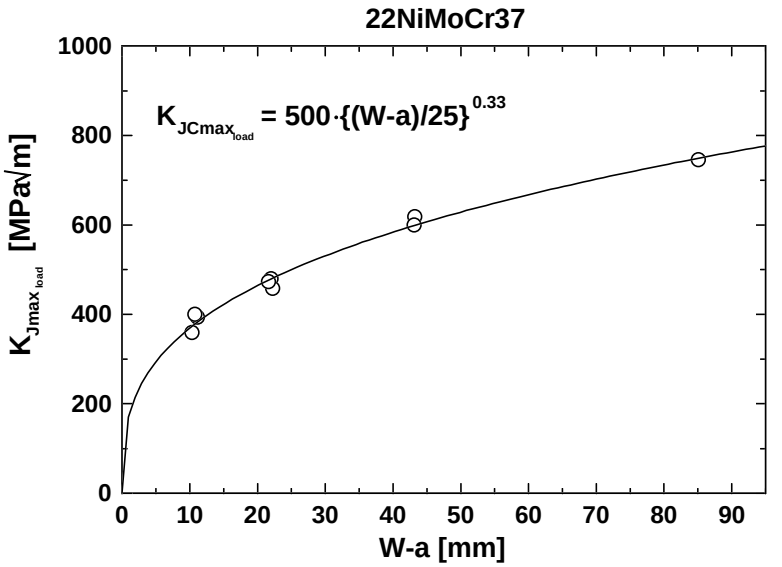

Figure 9. K_J at ductile maximum load as a function of specimen ligament size.

Some testing standards which recognise the maximum load fracture toughness (e.g. BS 7448) demand the use of full thickness specimens, but allow specimens with different ligament size. This is clearly wrong. For standard type bend specimens, the controlling dimension of the specimen is the ligament and not the thickness. The smaller the specimen ligament is the smaller the maximum load fracture toughness will be. Therefore, the demand for full thickness specimens is inappropriate.

3.5 Empirical analysis

Before performing a detailed master curve analysis of the results, a simple empirical analysis was performed to check the overall behaviour of the data. First the data for the individual specimen sizes was plotted in logarithmic co-ordinates to check trends in temperature dependence and scatter (Fig. 10). A Least Square Fit was performed on the data to determine an approximate estimate of the mean fracture toughness behaviour (solid lines in Fig. 10). At this point no distinction was made between failure and non-failure data. Also, deterministic "lower bound" estimates were developed by drawing lower envelope lines to the data (dashed lines in Fig. 10). The behaviour of the four specimen sizes is very similar. In all cases the proportional scatter is seen to increase when going to higher temperatures. This can have three explanations: [1]at higher temperatures there may be a loss of constraint, increasing the scatter, [2]there may be a lower limiting fracture toughness K_{min} causing the proportional scatter in terms of K_{Jc} to be a function of the K_{Jc}/K_{min} ratio (Eq. 6) or [3]the master curve assumption of the scatter behaviour may be wrong. However, the similarity between the three large data sets (12.5 mm, 25 mm and 50 mm) indicate a specific fixed scatter dependence (difference between mean and lower bound estimates is similar). The difference between mean and lower bound estimates for the 100 mm thick specimens is less, but this is directly attributable to the smaller number of tested specimens (the deterministic lower bound corresponds to a higher probability level). Explanations one and two appear most likely, operating separately or in combination.

The mean and lower bound curves are compared in Fig. 11. The mean curves show a clear size effect. The effect of increasing the specimen size is essentially to shift the curves higher in temperature. The shape of the mean curves appears

practically unaffected by specimen size. A doubling of specimen size seems equivalent to a constant temperature shift of approximately 9°C. Specimen size effects are less clear for the lower bound curves, but this may to some extent be due to their higher inherent uncertainty. Also the fact that the 100 mm thickness lower bound seem to coincide with the 12.5 mm thickness lower bound is (at least partly) due to the lesser number of 100 thickness specimens. Otherwise the results show the expected trend of decreasing lower bound toughness with increasing specimen size.

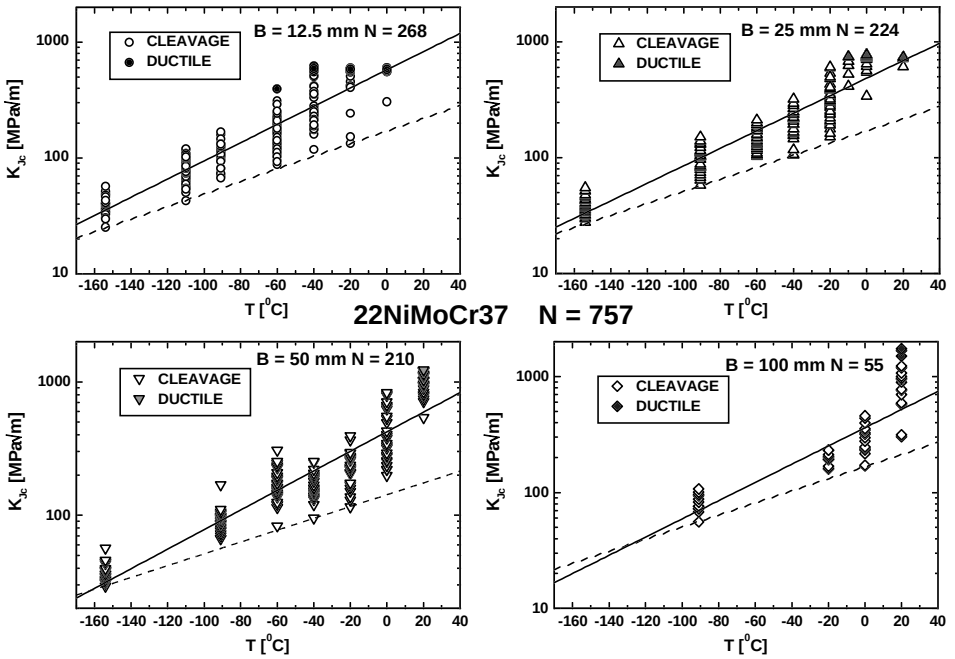

Figure 10. Individual specimen size fracture toughness results expressed in logarithmic co-ordinates. Solid lines are LSF mean estimates using all specimens (including non-failures) and dashed lines are "eye ball" deterministic lower bound estimates.

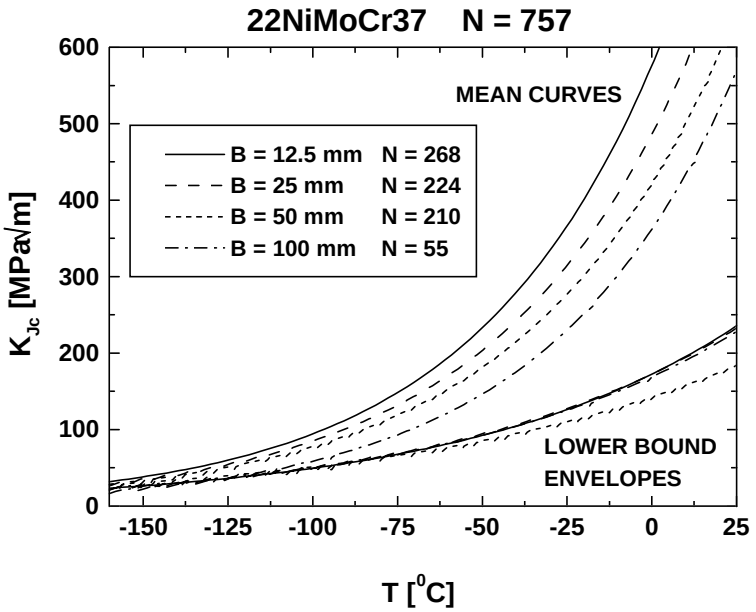

Figure 11. Comparison of LSF mean and "eye ball" lower bound fracture toughness estimates.

The simple mean estimates were compared with a master curve prediction of the median fracture toughness using a T_0 of -95°C (Fig. 12a).

The LSF mean curve estimates and the master curve predictions are clearly similar. The size effect is practically identical and also the curve shapes are similar. Small differences in the shape are to be expected, since the LSF mean predictions used a simple exponential function, extrapolating down to zero fracture toughness. The master curve assumes a slightly more advanced form of exponential function utilising an absolute lower shelf value of fracture toughness. Therefore, at low temperatures, the master curve prediction will be higher than the LSF mean estimate and, consequently, the reverse will be the case at high temperatures since the master curves were located to describe the average behaviour of the LSF estimates.

The comparison was repeated for the deterministic lower bound curves. They were compared with the 1% (and 5% for the 100 mm specimens) predictions of the master curve (Fig. 12b). In this case, the master curve seems to predict a larger size effect than shown by the deterministic curves. Actually the 12.5 mm,

25 mm and 100 mm lower bound curves are almost identical. This finding may be somewhat misleading. The number of 100 mm specimens is less than ¼ of the small specimens. Thus, the 100 mm deterministic lower bound is likely to correspond to a higher probability level (4 times) than for the others. The fact that the 5% master curve describes the 100 mm lower bound quite well indicates that 1% (or slightly higher) probability master curves should describe the smaller specimen lower bounds. Considering the uncertainty of deterministic lower bound curves, the results appear quite promising. No clear discrepancies with the master curve assumption is seen.

The empirical preliminary analysis indicates promise of having success with a detailed analysis of the data applying the master curve analysis method described in chapter 1. Thus, such an analysis is attempted next.

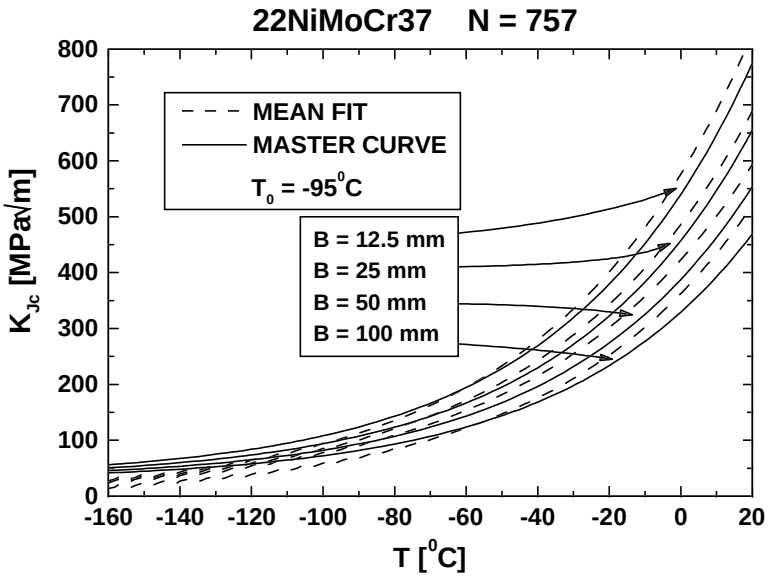

Figure 12a. Comparison of LSF mean estimates and the master curve median predictions using T_0 = -95°C.

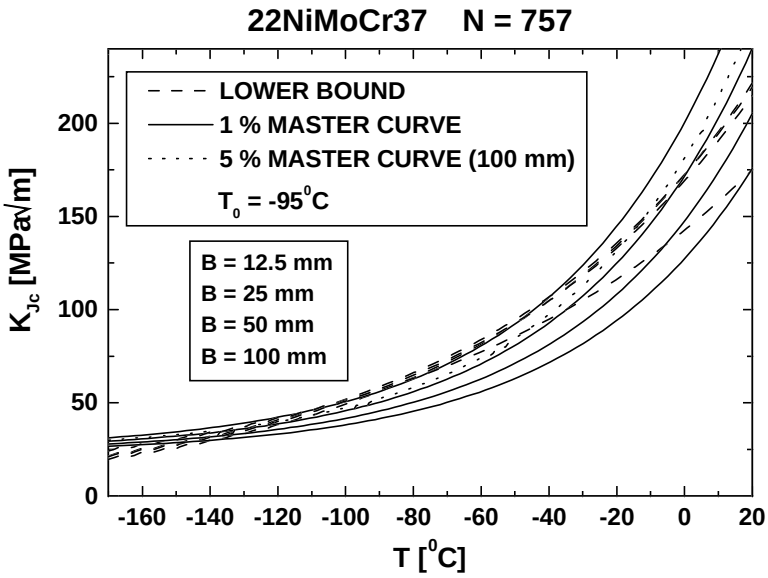

Figure 12b. Comparison of deterministic lower bound estimates and the master curve 1% (& 5%) lower bound predictions using T_0 = -95°C.

4. Master curve analysis

The master curve analysis is first discussed separately for each test temperature and subsequently an overall synthesis is made. The statistical size adjustment (Eq. 8) is not performed for the analysis of the different test temperatures, but only for the synthesis analysis.

4.1 T = -154°C

The temperature -154°C corresponds to the lower shelf region of fracture toughness. From the fracture surfaces this could be seen as a lack of single initiation sites. At this temperature the lower shelf behaviour depicted in Fig. 13 was seen for all but one specimen of 12.5 mm thickness. At higher temperatures the transition region (Fig. 13) behaviour became more and more dominant, starting with the smaller specimen sizes. This behaviour is well in accordance with the master curve assumption of the lower shelf and transition region fracture micromechanisms. The initiation site behaviour is further discussed in the synthesis section.

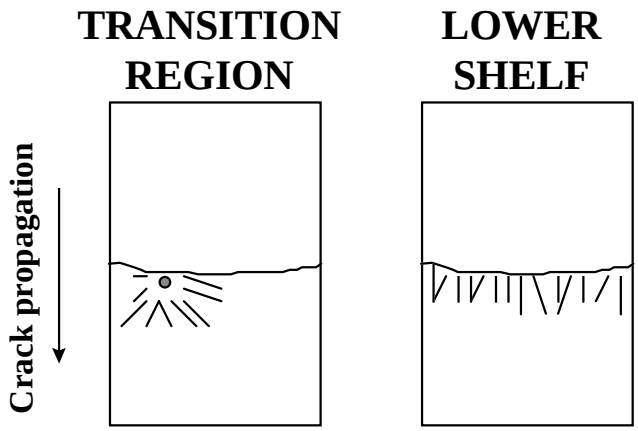

Figure 13. Typical cleavage fracture surfaces for fatigue precracked specimens.

The non-size-adjusted -154°C test results are presented in Figs 14–16 for specimen thickness 12.5 mm, 25 mm and 50 mm, respectively. All three cases are strikingly similar. The standard master curve description, with a fixed K_{min},

does not provide a very good description of the data, but this is expected, since the standard master curve is not supposed to work on the lower shelf. A slightly better description of the data is obtained with the master curve description, fitting also K_{min}, but clearly the best result is obtained with the expression developed specifically for the lower shelf (Eq. 12). The lower shelf expression correctly models the curvature seen in the data when plotted in master curve failure probability diagram co-ordinates. Hardly any size effect is visible in the results and, overall, there are no significant differences between the three data sets. The success of the lower shelf expression in describing the data and the fact that the fracture surfaces lack single initiation sites are strong evidence for the validity of the master curve assumption regarding the fracture mechanism on the lower shelf.

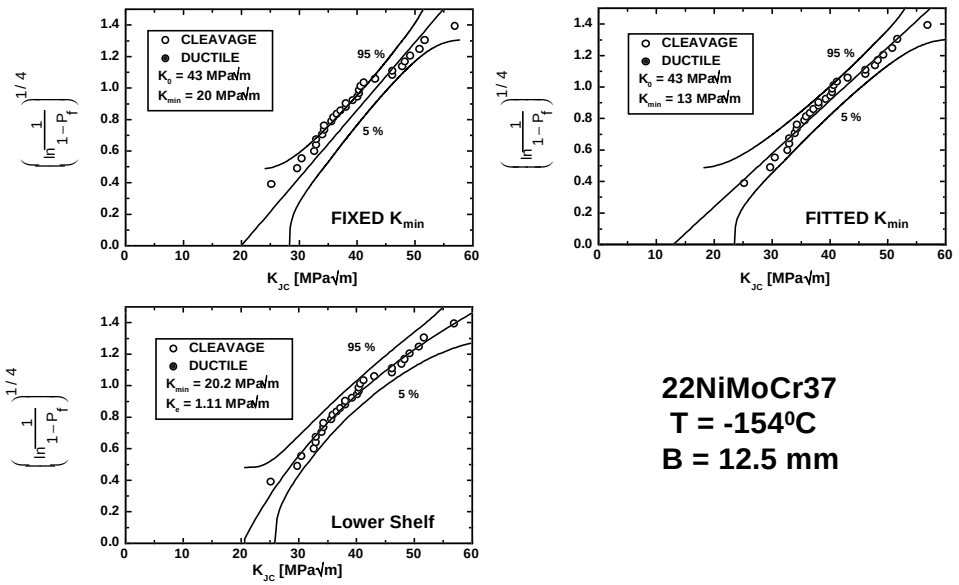

Figure 14. Failure probability diagram for 12.5 mm thick specimens at T = -154°C.

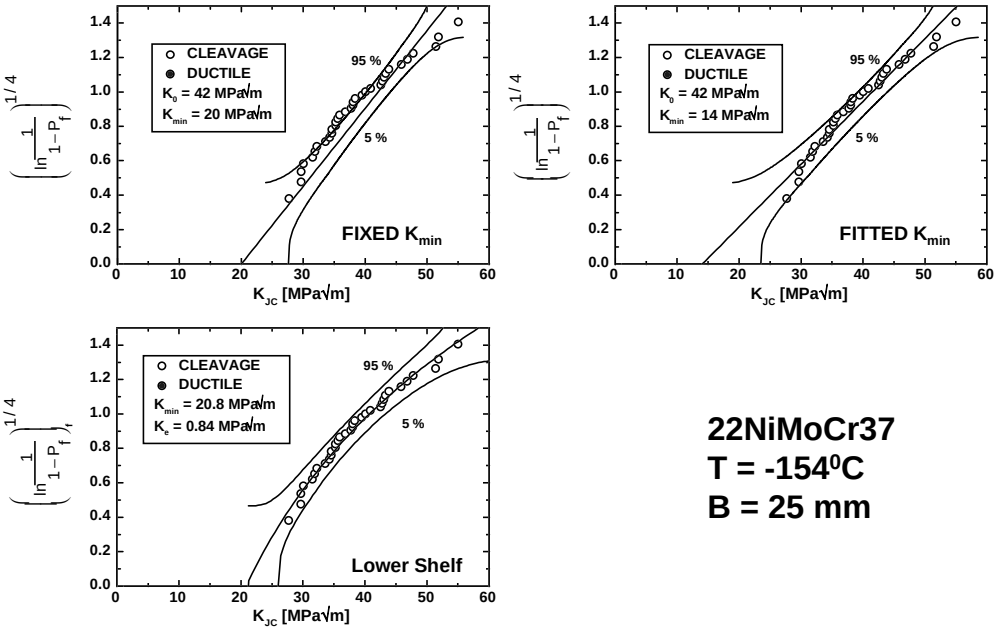

Figure 15. Failure probability diagram for 25 mm thick specimens at T = -154°C.

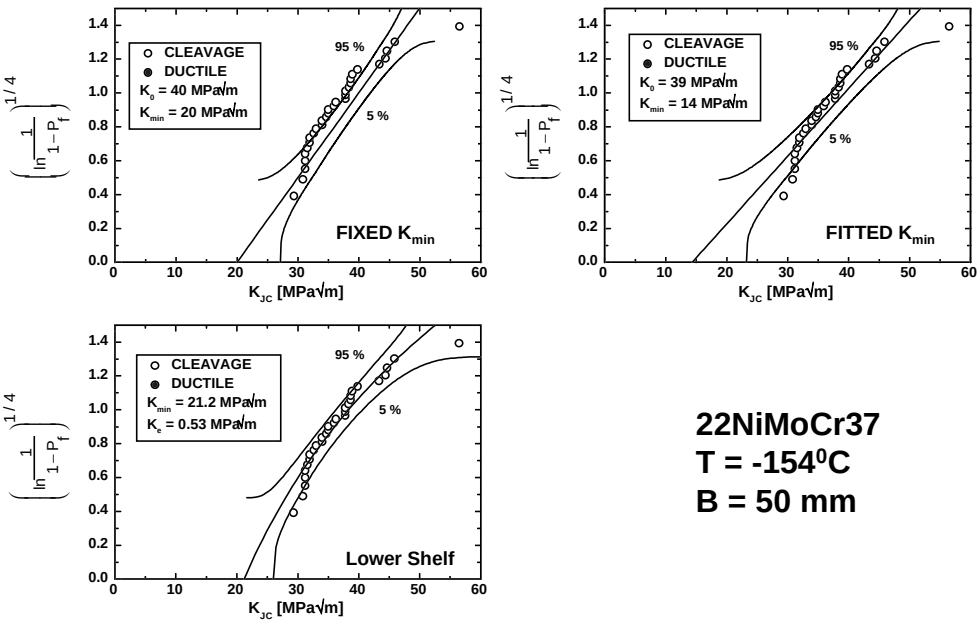

Figure 16. Failure probability diagram for 50 mm thick specimens at T = -154°C.

4.2 T = -110°C

The 55 tests at -110°C were performed as part of the materials pre-characterisation and therefore only one specimen size was used (12.5 mm thickness). Only 27% of the specimens lacked a single initiation site and therefore the basic master curve expression should work. The results are presented in Fig. 17. Using a fixed K_{min} or fitting does not make much difference. The fitted K_{min} is very close to the fixed value. Considering the large number of specimens in this data set, the result constitutes a strong validation of the assumed master curve scatter and K_{min}.

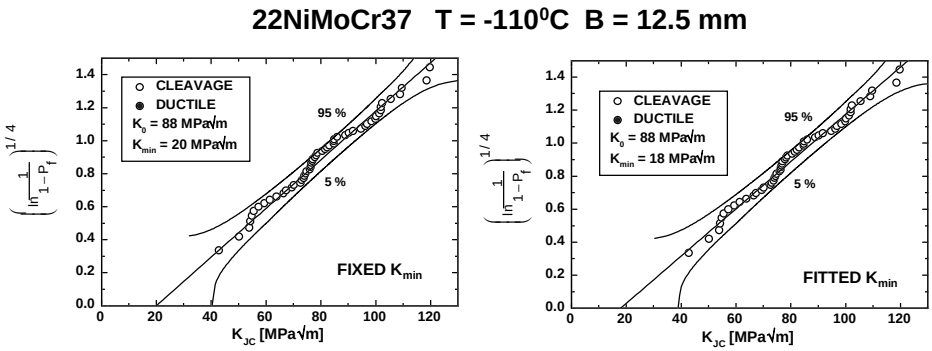

Figure 17. Failure probability diagram for 12.5 mm thick specimens at T = -110°C.

4.3 T = -91°C

All four specimen sizes were tested at -91°C and the non-size-adjusted results are presented in Figs 18–21. With the exception of the 100 mm specimens more than 50% of the specimens showed single initiation sites, so the weakest link based master curve expression should work. For the 100 thick specimens only one specimen showed a clearly recognisable single initiation site, so in this case lower shelf behaviour could be expected. This was not however supported by the fracture toughness behaviour (Fig. 21) which follows the master curve prediction very well. The discrepancy may be due to the difficulty of recognising initiation sites correctly on large fracture surfaces. Overall, however, the results show the expected size effect and scatter. The 50 mm thick

specimens do not quite confirm the expected scatter, but this may be due to a macroscopic inhomogeneity in the material used for the 50 mm specimens (verified for tests at -60°C) or to a statistical sampling effect (30 specimens is still small sample statistics). Most importantly, the standard master curve is shown to produce a realistic or conservative description of the data. The fitted K_{min} values are in all cases close to the fixed standard master curve value of K_{min} = 20 MPa√m.

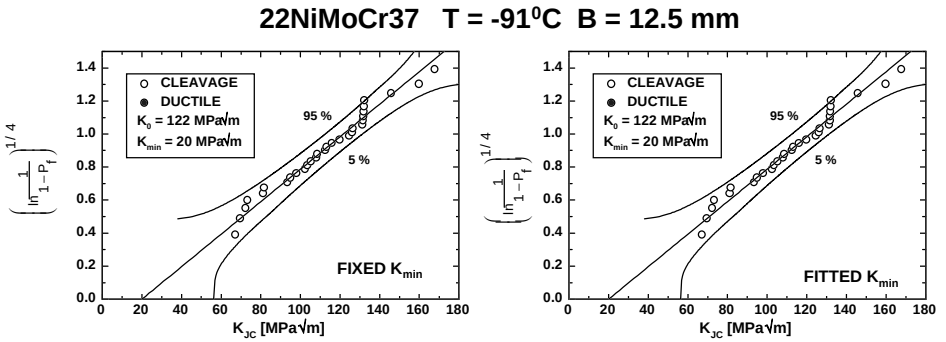

Figure 18. Failure probability diagram for 12.5 mm thick specimens at T = -91°C.

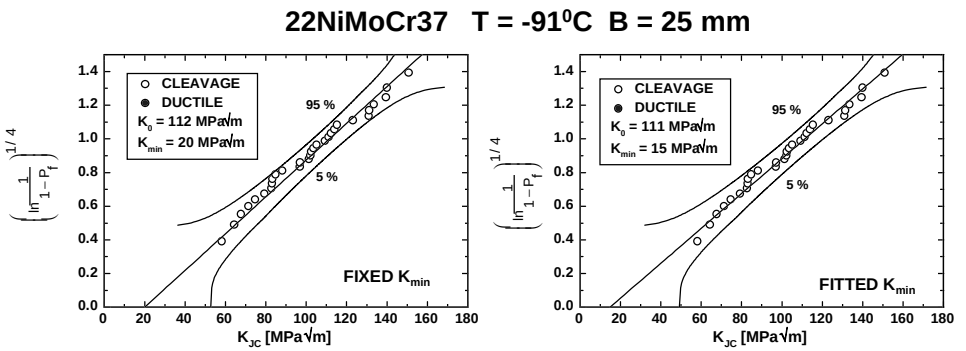

Figure 19. Failure probability diagram for 25 mm thick specimens at T = -91°C.

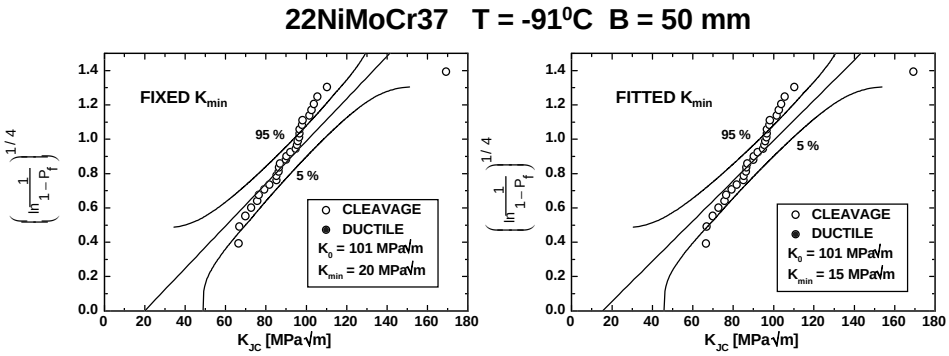

Figure 20. Failure probability diagram for 50 mm thick specimens at T = -91°C.

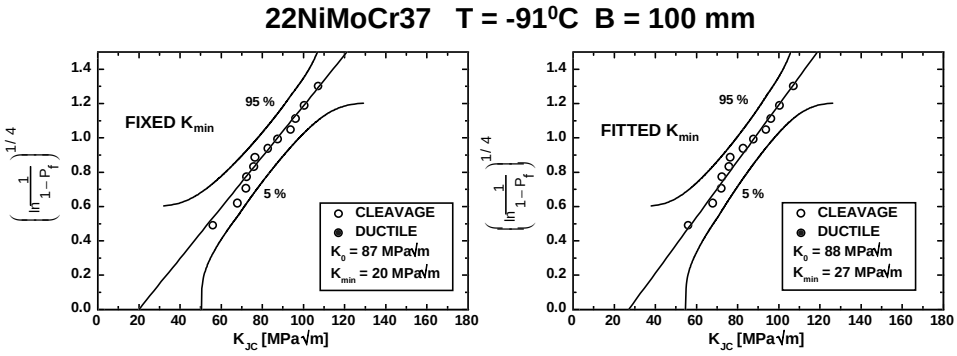

Figure 21. Failure probability diagram for 100 mm thick specimens at T = -91°C.

4.4 T = -60°C

Three smallest specimen sizes were tested at -60°C and the non-size-adjusted results are presented in Figs 22–24. Only for the 50 mm thick specimens, there were 40% specimens showing lack of single initiation sites. Thus the basic master curve expression should work. All sets follow the predicted distribution quite well. At this temperature the 12.5 mm thick specimens start to reach fracture toughness values in excess of the size requirement (Eq. 7). A loss of specimen constraint should be visible as a deviation towards the right from the straight line. Such a deviation does not occur before the M = 30 line, thus providing validation for the standard size requirement.

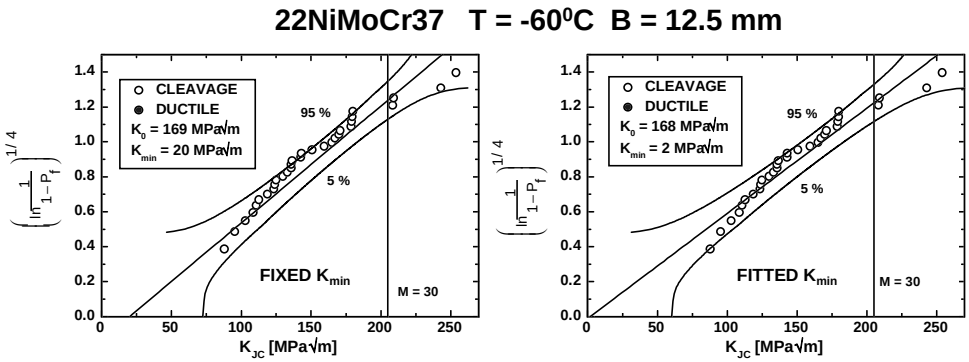

Figure 22. Failure probability diagram for 12.5 mm thick specimens at T = -60°C.

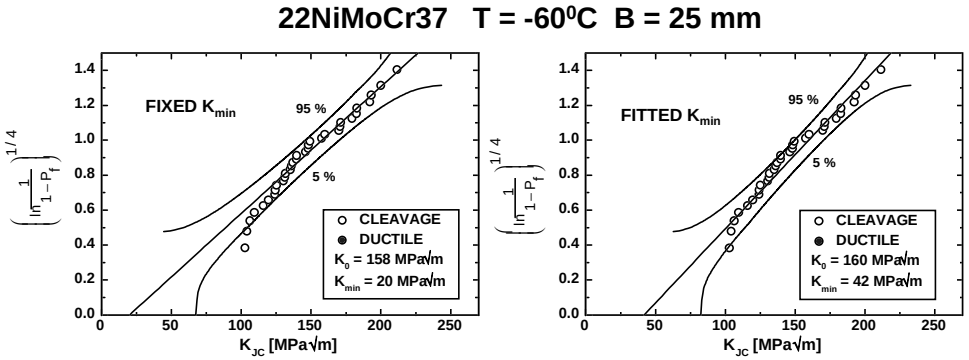

Figure 23. Failure probability diagram for 25 mm thick specimens at T = -60°C.

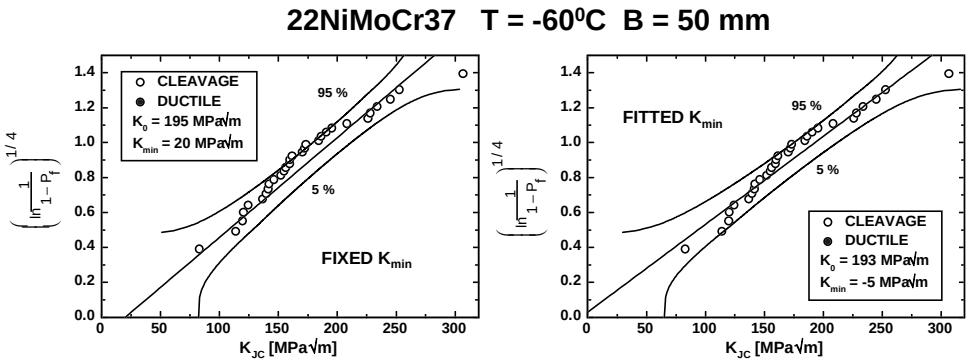

Figure 24. Failure probability diagram for 50 mm thick specimens at T = -60°C.

Even though the scatter and specimen measuring capacity appear to be according to the master curve assumptions, the same is not the case for the expected size effect. There is a decrease in K_0 going from 12.5 mm thickness to 25 mm, but the 50 mm thick specimens show a clearly higher toughness than the smaller specimens. This is not in accordance with weakest link behaviour, nor is it explainable by constraint speculations. The most logical reason for the behaviour is a macroscopic material variability. To check this possibility, GKSS manufactured and tested 30 additional 12.5 mm thick specimens, made from the broken 50 mm thick specimen halves. These "extra" results are presented in Fig. 25. The K_0 for the "extra" results is significantly higher than for the original 25.5 mm thick specimens. It is also higher than the K_0 for the 50 mm thick specimens. Thus the result tends to confirm the existence of a macroscopic material variability. The measuring capacity of the specimens appears again to be better than M = 30 indicates.

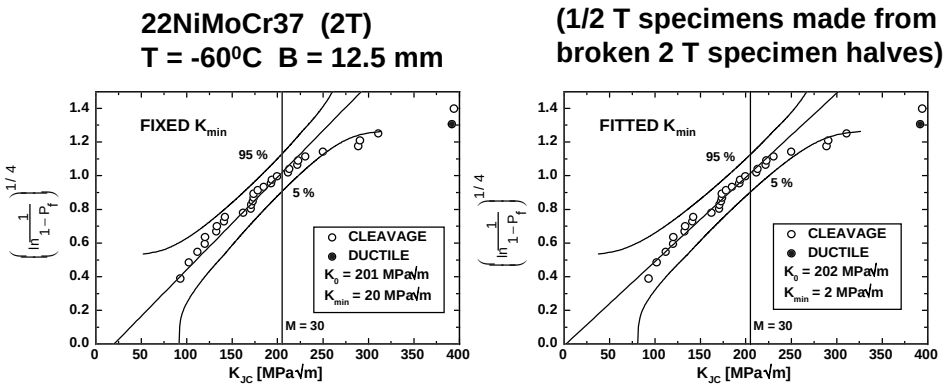

Figure 25. Failure probability diagram for 12.5 mm thick specimens at T = -60°C, made from broken 50 mm thick specimen halves.

To further investigate the origin of the inhomogeneity, the data was divided into two sets, one set containing data from sections SX2 and SX10 and one set containing data form section SX9. SX10 is the same section as used for the original 12.5 mm and 25 mm thick specimens. SX2 was used for 50 mm thick specimens tested at several different temperatures, not showing "anomalous" behaviour. The results are presented in Fig. 26 for the 50 mm thick specimens and Fig. 27 for the "extra" 12.5 mm specimens.

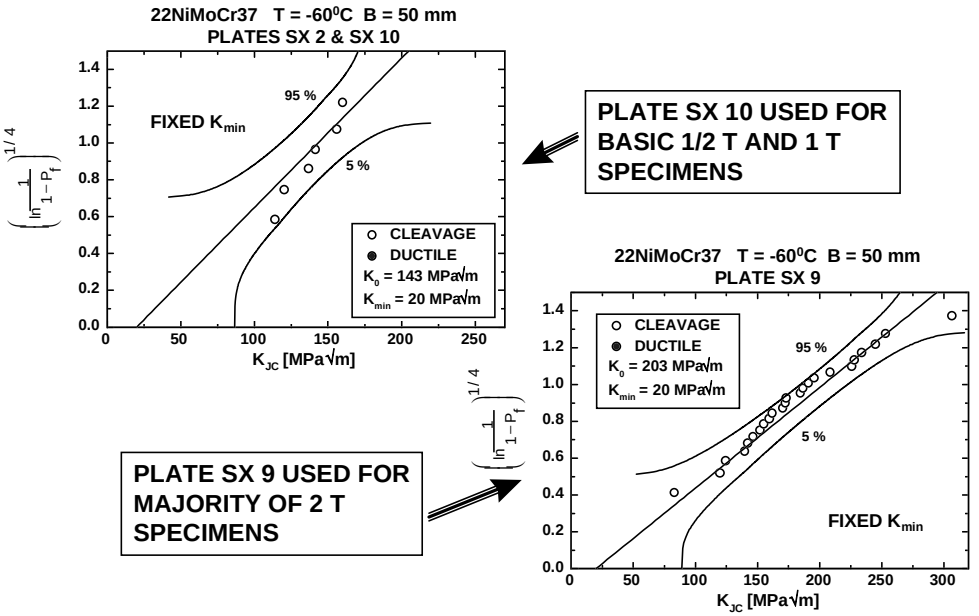

Figure 26. Failure probability diagram for 50 mm thick specimens at T = -60°C, ordered by plate.

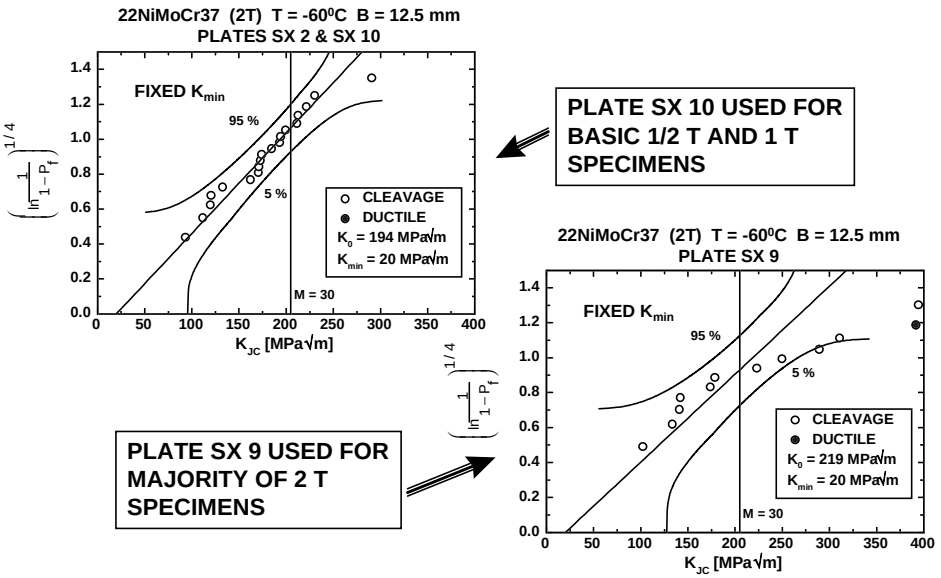

Figure 27. Failure probability diagram for 12.5 mm thick specimens at T = -60°C, made from broken 50 mm thick specimen halves, ordered by plate.

The trends are clear. The toughness of section SX9 is approximately 20% higher than for the neighbouring sections SX2 and SX10. This result indicates that also the other 50 mm thick specimen data sets may be affected by material variability. Finding this kind of a moderate material variability in such a big forging, is by no means unexpected. Actually, the found material variability is almost surprisingly small. The effect of the material variability on T_0 is further studied in the synthesis analysis.

4.5 T = -40°C

Three smallest specimen sizes were tested at -40°C and the non-size-adjusted results are presented in Figs 28–30. Only for the 25 mm thick specimens, there were 25% specimens showing lack of single initiation sites. Thus the basic master curve expression should work. All sets follow the predicted distribution quite well. At this temperature also the 25 mm thick specimens start to reach fracture toughness values in excess of the size requirement (Eq. 7). A deviation from the straight line behaviour does occur well beyond the M = 30 line, thus providing additional validation for the standard size requirement. The data show also a clear size effect. The size effect appears larger than for the lower temperatures, but this is at least partly apparent. The size effect should scale with (K_0-K_{min}) which indicates larger size effect at higher toughness levels. The test results seem to verify this trend.

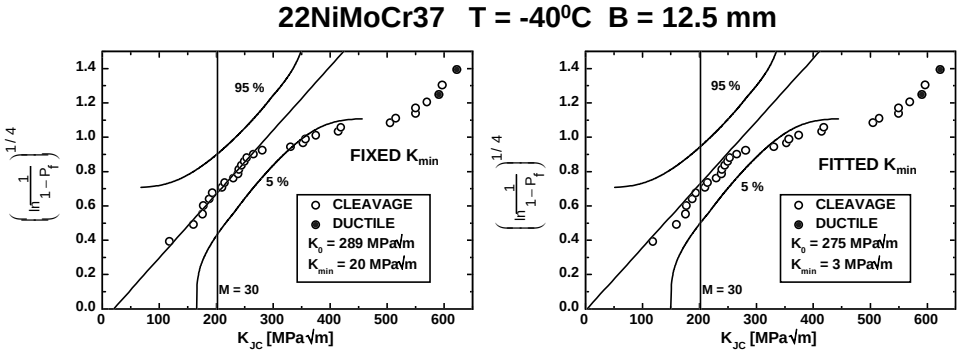

Figure 28. Failure probability diagram for 12.5 mm thick specimens at T = -40°C.

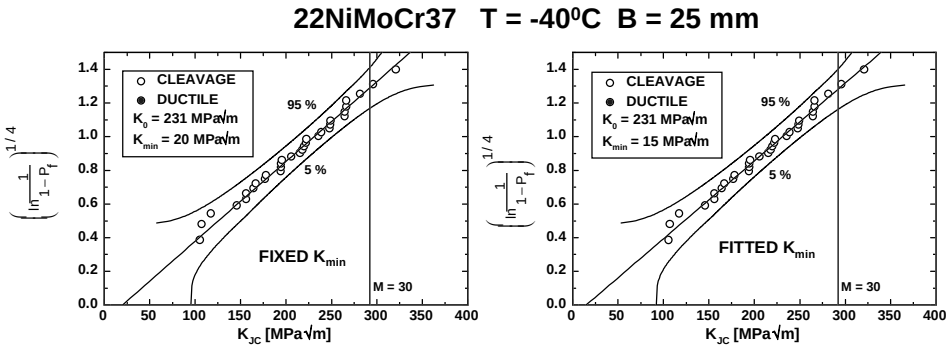

Figure 29. Failure probability diagram for 25 mm thick specimens at T = -40°C.

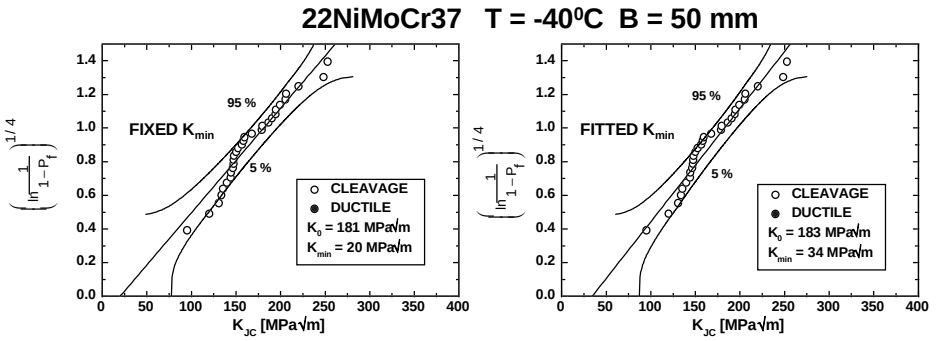

Figure 30. Failure probability diagram for 50 mm thick specimens at T = -40°C.

4.6 T = -20°C

All four specimen sizes were tested at -20°C and the non-size-adjusted results are presented in Figs 31–34. The basic master curve expression should work for all specimen sizes. At this temperature, nearly all of the 12.5 mm thick specimens (Fig. 31) reach fracture toughness values in excess of the size requirement (all but 2) and also the number of non-failures (ductile end-of-tests) is considerable. In this case, the fitted K_{min} estimate is meaningless, and also the K_0 estimate, even for the fixed K_0 case is unreliable. It does, however, appear that loss of constraint becomes significant only above the M = 30 toughness criterion. The 25 mm and 50 mm thick specimens (Figs 32 and 33) follow the

master curve assumptions nicely and provide also additional verification for the validity of the standard size requirement.

The 100 mm thick specimens (Fig. 34), indicate a higher K_{min} value, but also the standard value is possible considering the confidence of the K_{min} estimate.

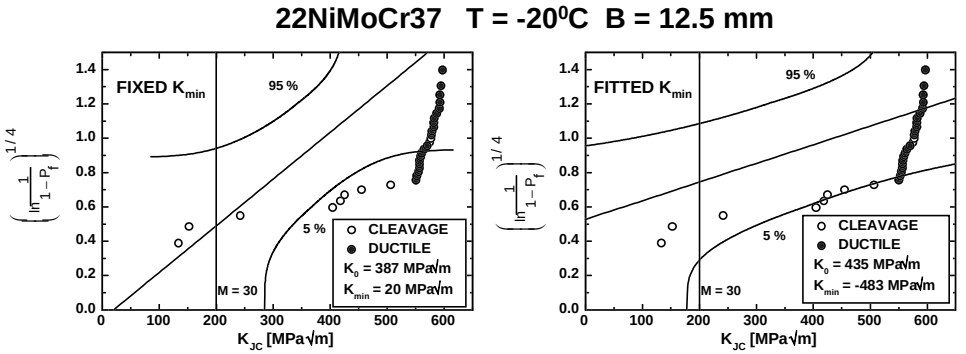

Figure 31. Failure probability diagram for 12.5 mm thick specimens at T = -20°C.

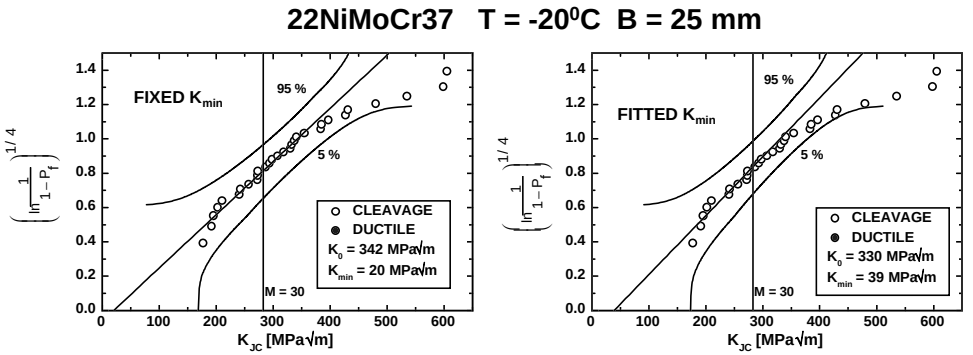

Figure 32. Failure probability diagram for 25 mm thick specimens at T = -20°C.

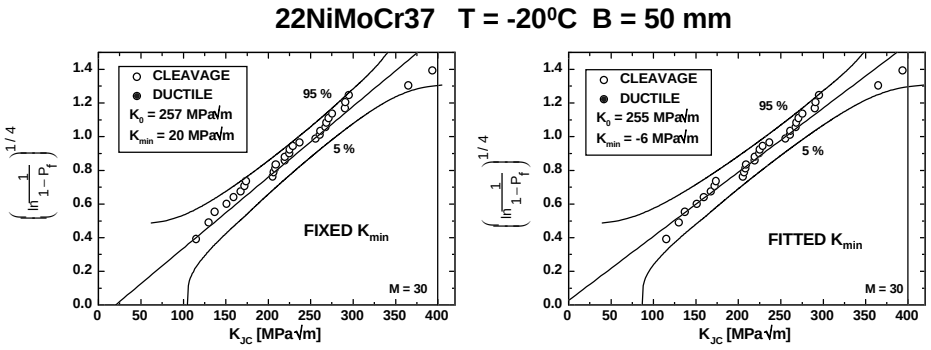

Figure 33. Failure probability diagram for 50 mm thick specimens at T = -20°C.

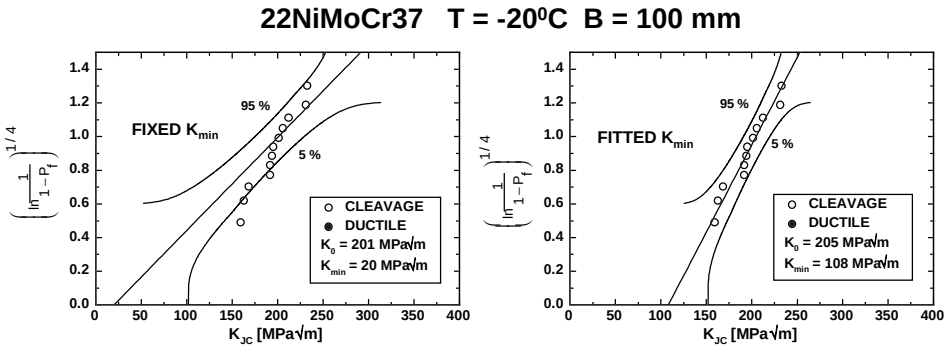

Figure 34. Failure probability diagram for 100 mm thick specimens at T = -20°C.

Additionally 20, side-grooved, specimens were manufactured and tested at this temperature. The specimens had standard 10% side-grooves on both sides and the results are presented in Fig. 35. The side grooved specimens provide a 7% lower value than the non-side-grooved specimens (Fig. 32). The expected standard deviation (Eq. 6) of the respective K_0 estimates are 8.4% (0% SG) and 9.3 (20% SG), which means that the found difference is not statistically significant. In order to compare the two specimen types in more detail, the 20 non-side-grooved specimens tested outside GKSS were compared directly with the 20 side-grooved specimens tested by the same laboratory. Both sets of data were ordered by rank and each of the corresponding data pairs (in principle corresponding to the same rank probability) were compared. The comparison is presented in Fig. 36. It should be pointed out that the uncertainty of the

comparison is √2-times bigger than for the individual analysis. Thus the observed difference of 10% (Fig. 36) is not statistically significant. More revealing is the overall trend in the data. The relation between the two specimens is linear almost up to ductile maximum load (see Fig. 9) after which the non-side-grooved values seem to deviate to higher toughness values. I.e. the both specimens show an identical constraint behaviour up to ductile maximum load. Finally, also the tearing resistance of the two specimen types were compared (Fig. 37). Based on a power law fit to the data, also here, the side-grooved specimens indicate a lower toughness than the non-side-grooved ones. The difference is clearer for the post maximum load values, but there appears to be a slight difference also for lower toughness values. Thus, the ductile tearing results are in agreement with the brittle fracture behaviour. Side-grooves produce a slightly more conservative result.

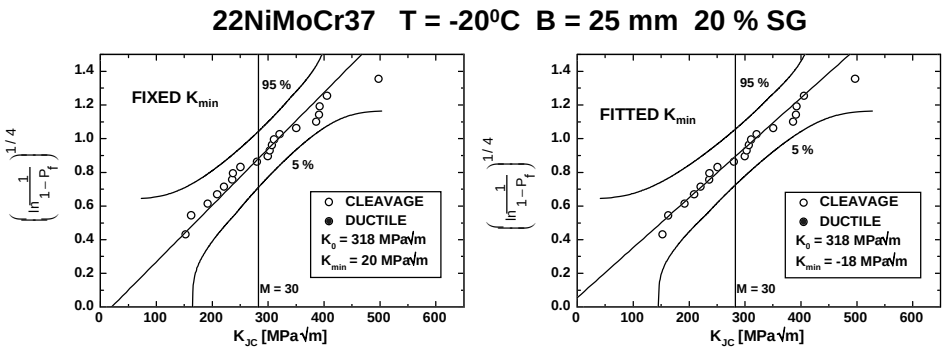

Figure 35. Failure probability diagram for 25 mm thick specimens, with 20% side-grooving, at T = -20°C.

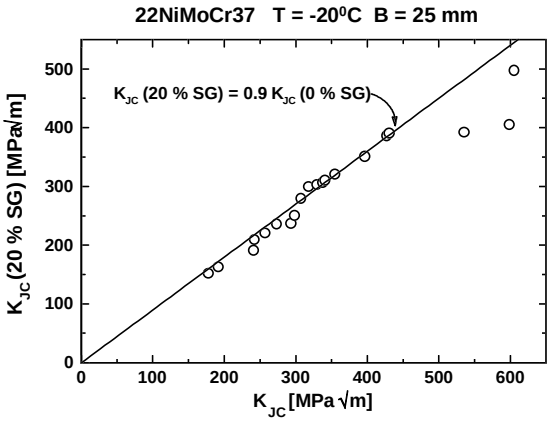

Figure 36. Comparison between fracture toughness of side-grooved and non-side-grooved 25 mm thick specimens at -20°C.

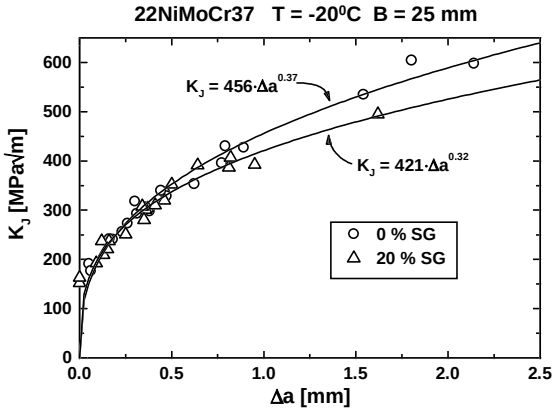

Figure 37. Comparison between tearing resistance of side-grooved and non-side-grooved 25 mm thick specimens at -20°C.

4.7 T = -10°C

At -10°C only five 25 mm thick specimens were tested to check that upper shelf behaviour would not be encountered earlier than predicted. The results are presented in Fig. 38. No valid results were obtained, so a master curve interpretation of the results was not pursued. Only one of the five specimens did not cleave, so it was decided to continue to increase the testing temperature still.

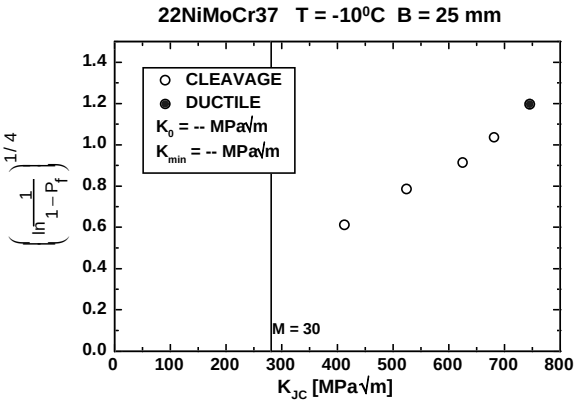

Figure 38. Failure probability diagram for 25 mm thick specimens at T = -10°C.

4.8 T = 0°C

All four specimen sizes were tested at 0°C. The non-size-adjusted results are presented in Figs 39–42. As expected, the 12.5 mm and 25 mm thick specimens did not provide any results fulfilling the specimen size criterion (Figs 39 and 40). Thus, for these specimens a master curve analysis was not applicable. More than half of the 50 mm thick specimens (Fig. 41) and all 100 mm specimens (Fig. 42) fulfilled the size criterion, so for these cases the master curve expression should work. The 50 mm specimens seem to loose constraint above M = 30 whereas the 100 mm specimens all follow nicely the predicted behaviour. A size effect is also clearly present. In order to get an understanding of the amount of loss of constraint for the smaller specimens, a prediction based on the 100 mm specimen behaviour was made for these sets (Figs 39 and 40). Clearly, the small specimens have been affected by a loss of constraint, so data sets where all specimens violate the size criterion should obviously not be used for determining the master curve.

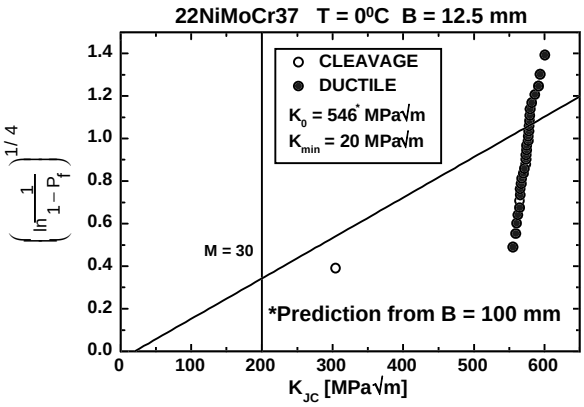

Figure 39. Failure probability diagram for 12.5 mm thick specimens at T = 0°C.

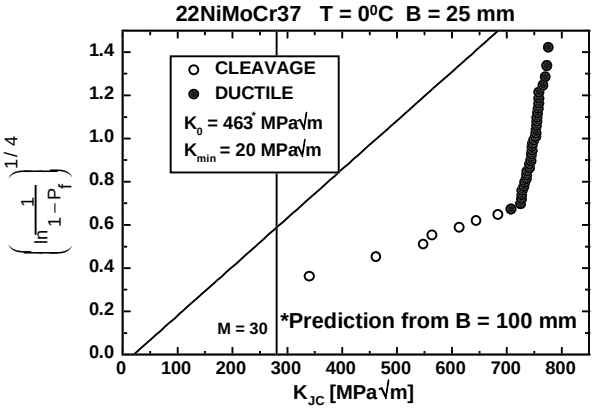

Figure 40. Failure probability diagram for 25 mm thick specimens at T = 0°C.

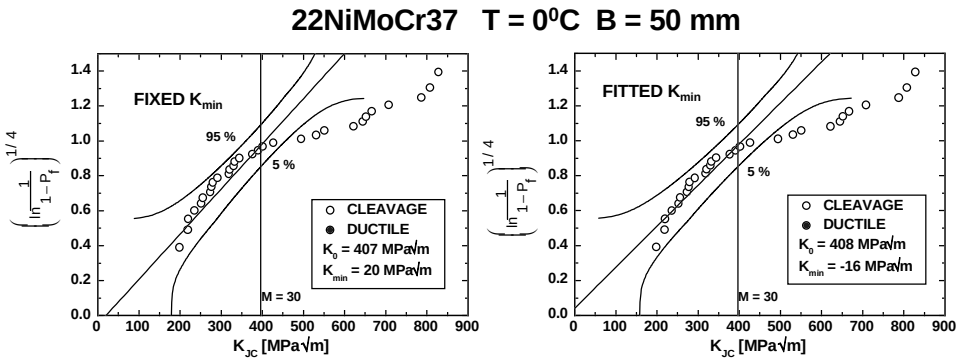

Figure 41. Failure probability diagram for 50 mm thick specimens at T = 0°C.

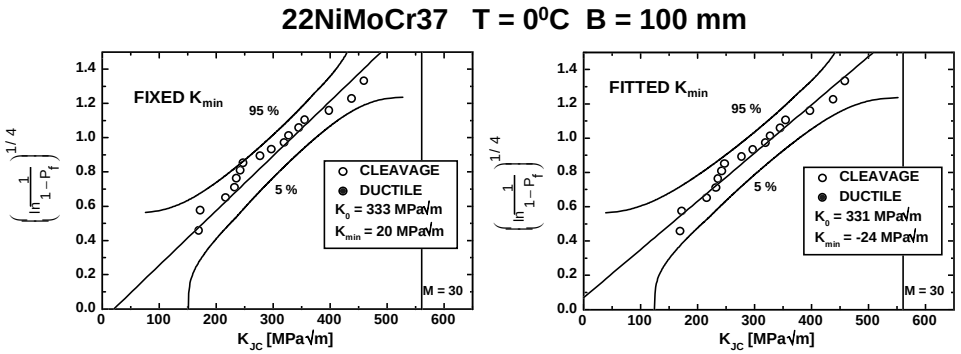

Figure 42. Failure probability diagram for 100 mm thick specimens at T = 0°C.

4.9 T = +20°C

The final test temperature was +20°C where the three largest specimen sizes were tested. The non-size-adjusted results are presented in Figs 43–45. Neither 25 mm nor 50 mm specimens were able to provide any values fulfilling the size requirement and a master curve analysis was therefore not applicable. The 100 mm thick specimens had all but two values in excess of the size requirement. Thus, the fitted K_{min} estimate is meaningless, and also the K_0 estimate, even for the fixed K_0 case is unreliable. The results do, however, imply that loss of constraint becomes significant only above the M = 30 toughness criterion.

The results show also another significant aspect, related to the existence of a "upper shelf" transition temperature. The results show that cleavage fracture initiation is possible at very high K_{Jc}-values and at high temperatures. No absolute "upper shelf" transition temperature was found. Thus, the master curve assumption that the brittle to ductile transition is nothing else than a combination of two separate fracture mechanisms is supported by the present results. The brittle to ductile transition is not a true material property. It is always related to the structural size. A large structure, allowing for much ductile crack growth will have a higher transition temperature than a smaller structure of the same material and this is true even if the constraint of the structures is the same. Any definition of an upper shelf transition temperature should be based on a constant specimen geometry and size. And it should be recognised that this transition temperature will be different for a real structure.

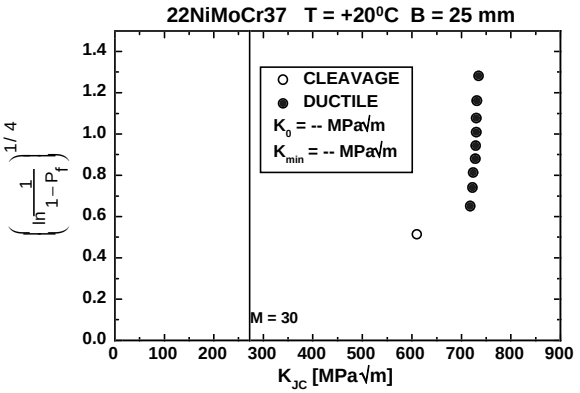

Figure 43. Failure probability diagram for 25 mm thick specimens at T = +20°C.

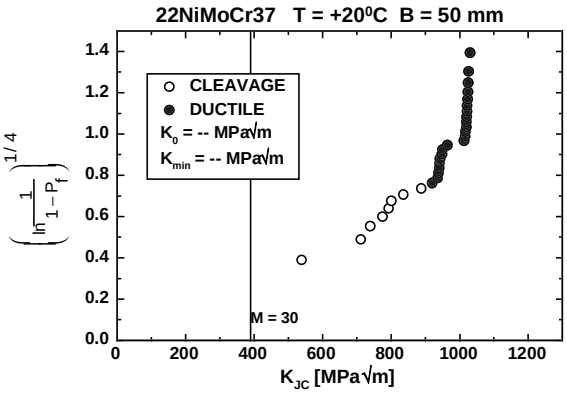

Figure 44. Failure probability diagram for 50 mm thick specimens at T = +20°C.

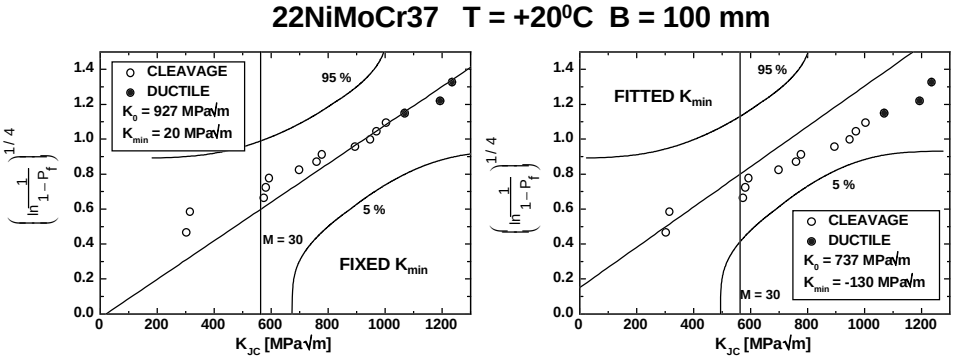

Figure 45. Failure probability diagram for 100 mm thick specimens at T = +20°C.

5. Synthesis analysis

The synthesis analysis will make an assessment, based on the master curve predictions, of the lower shelf behaviour of the initiation sites, the size effect of K_0, the temperature dependence of the master curve and the validity of a fixed K_{min} = 20 MPa√m assumption. Finally, an overall multi-temperature master curve analysis is made and recommendations for the applicability of the master curve are given.

5.1 Lower shelf behaviour

The lower shelf behaviour is studied by examining the percentage of specimens not showing single initiation sites on the fracture surface (Fig. 13). Two ways of presentation was selected: [1)]as a function test temperature and [2)]as a function K_0. The results are presented in Figs 46 a and b. When plotting the results against temperature there seems to be a clear size effect on the lower shelf behaviour (large specimens are more prone to show lower shelf behaviour than small specimens) and also the scatter is quite large. Plotting the results against K_0 removes some of the size effect and decreases the scatter.

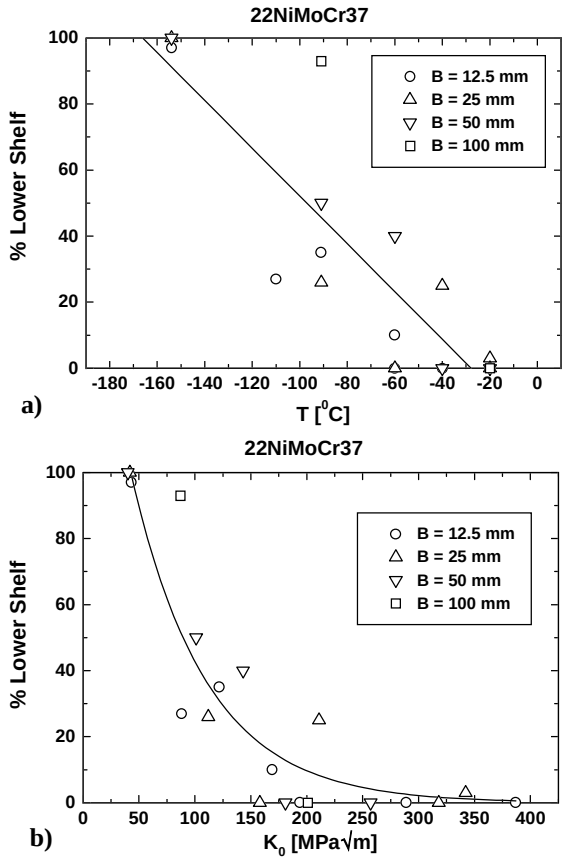

Figure 46. Percentage of specimens not showing single initiation sites as a function of a) temperature and b) K_0.

From the fracture toughness results it was clear that only the data sets showing practically 100% lower shelf behaviour on the fracture surface, also showed the expected scatter and lack of size effect. This is fully in line with the master curve assumptions. Close to the lower shelf, initiation will for some specimens be much easier than propagation and these specimens will show lower shelf type fracture surfaces. For other specimens propagation will be easier than initiation and these specimens will show single initiation sites on the fracture surface. Their overall distribution will however follow the standard master curve distribution, which includes the conditional propagation criterion (leading to non-zero K_{min}). Only when in all cases, the probability of propagation controls the fracture event, the lower shelf master curve distribution function will come

into effect. This means that fracture surface appearance can be used to choose distribution function. If any specimens at a specific temperature show single initiation sites, the scatter is likely to follow the standard master curve. Only if all specimens show lower shelf type fracture surfaces, the lower shelf master curve may be more appropriate (providing a sufficient number of tests have been performed N >> 6). If in doubt, the standard master curve distribution should be assumed.

5.2 Size effect of K_0

All the MML (fixed K_{min}) K_0 estimates were ordered by test temperature and plotted against specimen thickness and compared with the master curve size effect predictions (Fig. 47). In all cases the validity of the master curve size effect (Eq. 8) is confirmed quite clearly. This is true even for the lower shelf temperature (-154°C). I.e. even the standard master curve predicts negligible size effects on the lower shelf. Even more important is the finding that there is no trend for the smaller specimens to show a significantly larger size effect than predicted by the master curve. Even for the smallest specimens tested at -40°C and -20°C the predictions are within 10%, i.e. of the same order as the theoretical accuracy of the MML K_o estimate. Note that the 12.5 mm thick specimens at -20°C contained only 2 results fulfilling the size requirement. As many as 28 specimens were censored to correspond to the M = 30 value.

It appears that, at least for this type of materials, a size criterion of M = 30 is actually sufficient even for single specimen values as defined e.g. in ASTM E1820 or ESIS P2. Anyway, the results provide a very strong confirmation of the validity of the standard master curve size requirement of **M = 30**.

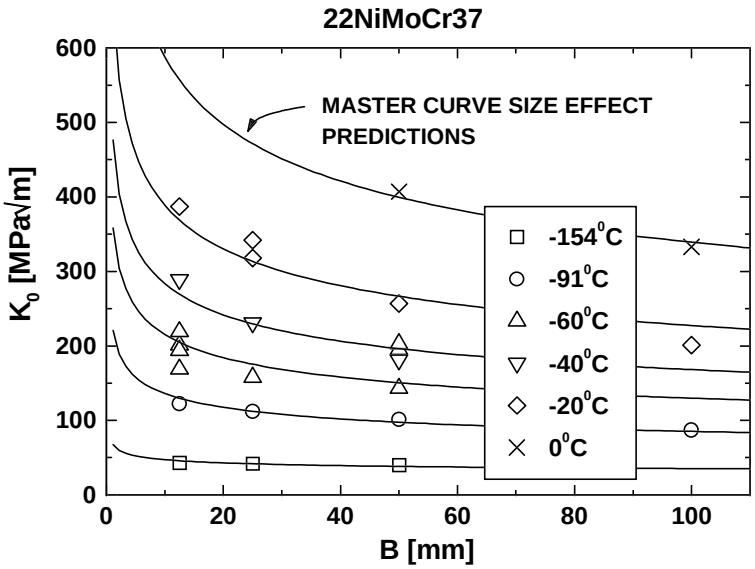

Figure 47. Size effect of MML estimated K_0 values compared with master curve predictions of the size effect.

5.3 Temperature dependence of K_0

The temperature dependence of the size adjusted (B_0 = 25 mm) K_0 values was compared with the standard master curve assumption. Two means of comparison were used. A direct comparison in terms of K_0 which is presented in Fig. 48 and an indirect comparison in terms of the calculated standard T_0 values which are presented in Figure 49. Into the comparison were included also the estimates corresponding to the separate plate SX9 and plates SX2 and SX10. This was made in order to include the effect of the "extreme" variability on the scatter of T_0.

With the exception of plate SX9 (at -60°C), all K_0 results show a very consistent behaviour. No systematic differences between different size specimens are present. A best fit of the same exponential form as the standard master curve provided a result very close to the standard master curve (Fig. 48). The main difference (proportionally) occurs on the lower shelf. For this material the master curve expression should therefore be slightly modified for the lower shelf. The standard master curve is, however, not meant to be applied blindly

down to lower shelf temperatures. If the lower shelf fracture toughness needs to be assessed, tests corresponding to lower shelf temperatures should be performed. The overall standard deviation of the T_0 estimates (not including the lower shelf results, but including plate SX9) is 6.7°C. Since the theoretical average standard deviation of the T_0 estimate is approximately 4°C, it means that the material related scatter is only 5°C, which, considering the amount of material sampled, is very little.

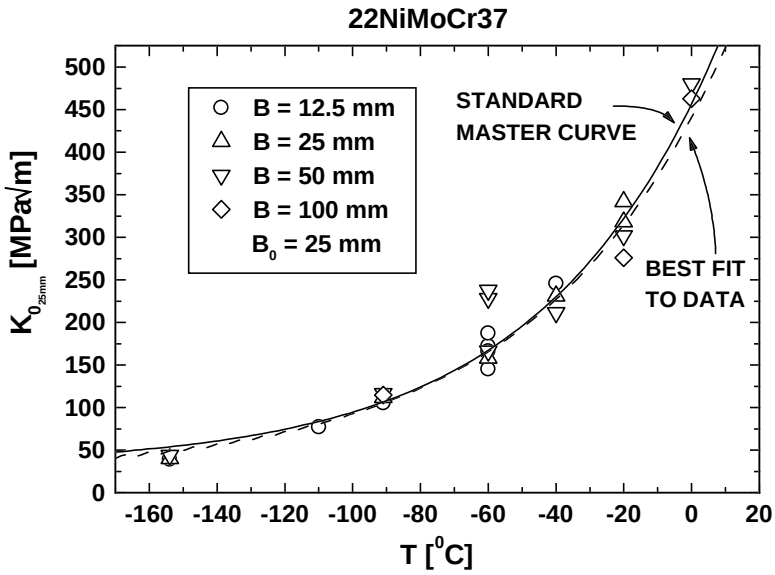

Figure 48. Temperature dependence of size adjusted K_0 values compared with standard master curve temperature dependence.

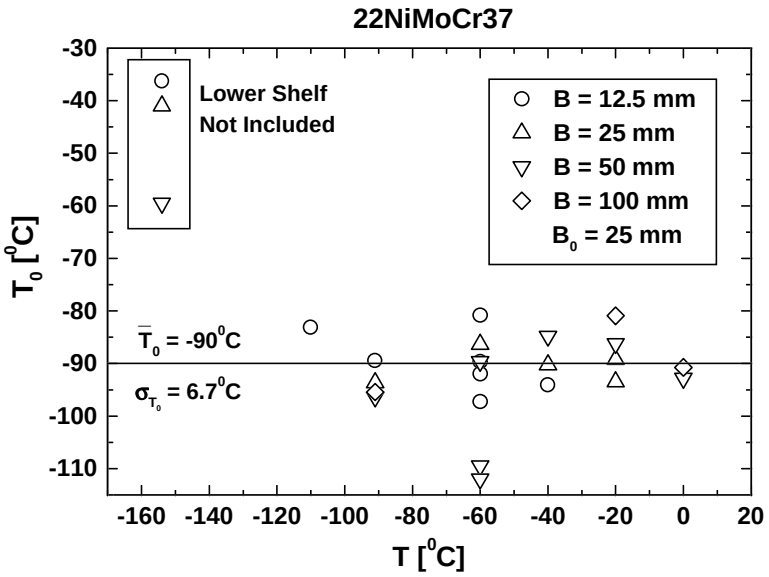

Figure 49. Comparison of T_0 estimates from the individual data sets.

5.4 Validity of fixed K_{min}

The validity of the assumption of a fixed value for the limiting fracture toughness (K_{min} = 20 MPa√m) was investigated by plotting the individual MML K_{min} estimates as a function of temperature (Fig. 50). The scatter in K_{min} increases with temperature (K_0), but this is as expected based on Fig. 4. The results were compared with the theoretical 5% and 95% confidence bounds for the MML estimate (Fig. 4) assuming a true value of 20 MPa√m. No trends with respect to specimen size nor temperature are visible. Thus, at least for this material, the assumption of a constant temperature independent K_{min} value close to 20 MPa√m is verified.

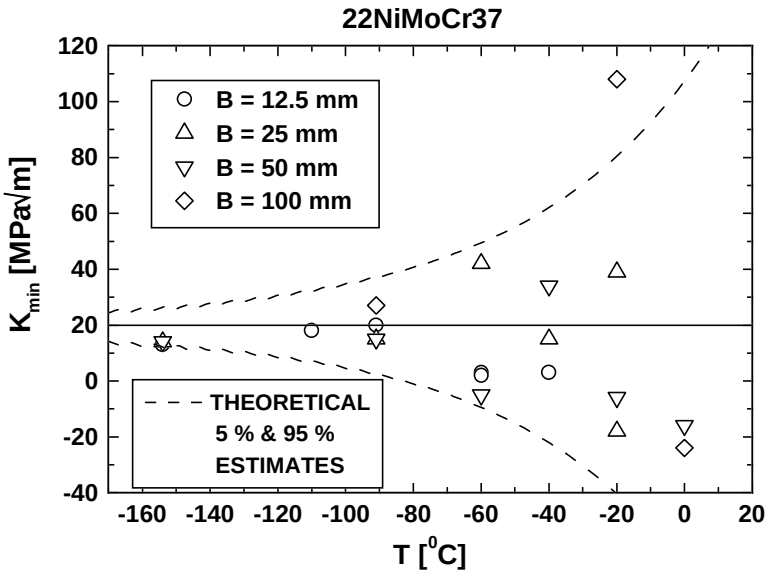

Figure 50. Temperature dependence and scatter of MML estimate of K_{min} compared to 5% and 95% confidence bounds for fixed K_{min} of 20 MPa√m

5.5 Multi-temperature master curve analysis

As a final check of the applicability of the master curve method, the different size specimen data were analysed by the multi-temperature T_0 MML algorithm (Eq. 10). The analysis results are presented in Figs 51–54a and b. Two different fits were made one applying all data (Figs 51–54 a) and one applying only data in the range $-50°C \leq T - T_0 \leq +100°C$ (Figs 51–54b). The T_0 estimates applying all data vary from -85°C down to -97°C. Applying only the central part of the data decreases the scatter in T_0 a little (-87°C…-97°C). The standard deviation in this case is 4°C, which is well in line with the expected material variability. There is an indication that the highest test temperature has a higher fracture toughness than predicted by the master curve. Thus, too low and too high test temperatures should be avoided for the estimation of T_0.

Based on the results, and previous theoretical estimates (Fig. 3), it seems advisable to limit the master curve T_0 estimation to testing temperatures in the range $-50°C \leq T - T_0 \leq +50°C$. Testing should include several temperatures

(preferably more than three), in order to minimise any effects from a possible deviation from the assumed temperature dependence.

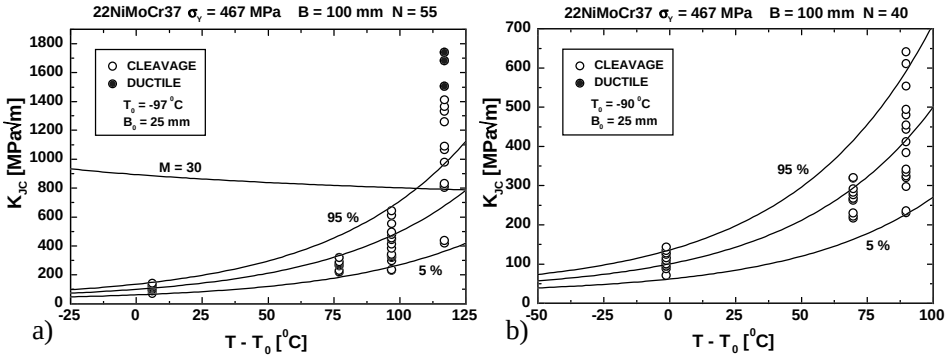

Figure 51. Multi-temperature MML T_0 analysis of 100 mm thick specimen data. a) using all data, b) using data in the range -50 °C ≤ T_0 ≤ +100 °C.

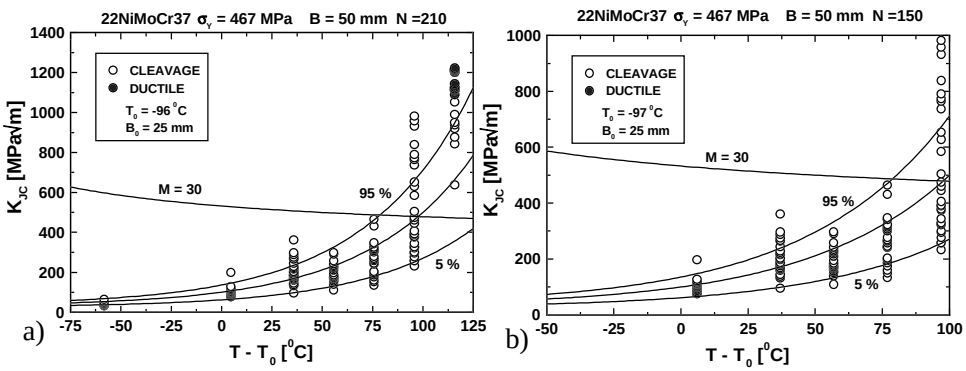

Figure 52. Multi-temperature MML T_0 analysis of 50 mm thick specimen data. a) using all data, b) using data in the range -50 °C ≤ T_0 ≤ +100 °C.

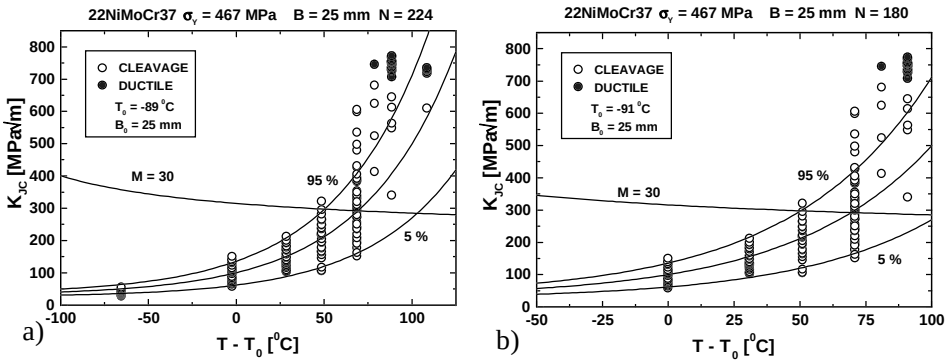

Figure 53. Multi-temperature MML T_0 analysis of 25 mm thick specimen data. a) using all data, b) using data in the range -50°C ≤ T_0 ≤ +100°C.

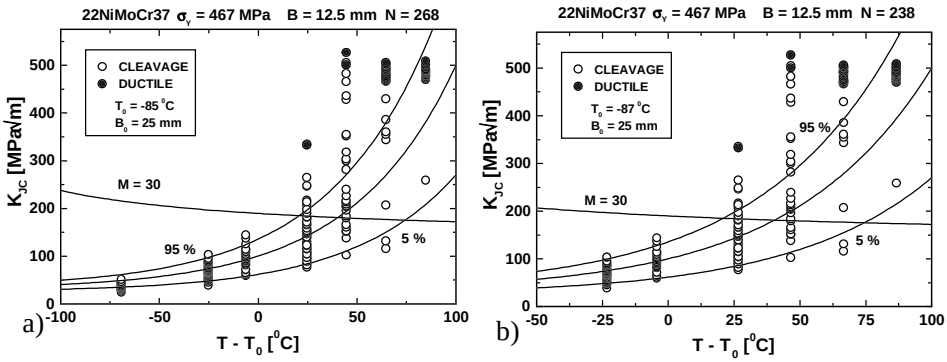

Figure 54. Multi-temperature MML T_0 analysis of 12.5 mm thick specimen data. a) using all data, b) using data in the range -50°C ≤ T_0 ≤ +100°C.

6. Summary and conclusions

A large nuclear grade pressure vessel forging 22NiMoCr37 (A508 Cl.3) has undergone extensive fracture toughness testing. The tests were performed on standard geometry CT-specimens having thickness 12.5 mm, 25 mm, 50 mm and 100 mm. The a/W-ratio was close to 0.6 for all specimens. One set of specimens was 20% side-grooved. A total of 757 results fulfilling the ESIS-P2 test method validity requirements with respect to pre-fatigue crack shape and the ASTM E-1921 pre-fatigue load, were obtained. The master curve statistical analysis method was applied extensively on the data, in order to verify the validity of the method. Based on the analysis the following can be concluded regarding the validity of the master curve method for this material:

1. The master curve scatter assumption is valid.

2. The master curve size effect assumption is valid.

3. The master curve temperature dependence assumption is valid.

4. The master curve minimum fracture toughness assumption is valid.

5. The master curve (E1921-98) specimen size requirement is valid.

6. The master curve lower shelf behaviour assumption is valid.

7. Lower shelf behaviour can be suspected if no specimens show single initiation sites on the fracture surface.

8. Determination of T_0 should be based on test results in the temperature range $-50°C \leq T - T_0 \leq +50°C$.

9. Testing should include several test temperatures, in order to minimise any effects from a possible small deviation from the master curve temperature dependence.

10. If only approximate (lower bound type) information regarding the fracture toughness is required, the master curve can well be extrapolated outside the range $-50°C \leq T - T_0 \leq +50°C$.

11. If an accurate description of the fracture toughness outside this temperature range is required, tests should preferably be performed at the specific temperature of interest. The master curve analysis method (excluding the temperature extrapolation) can be used also in this case for the description of scatter and size effects.

12. For side-grooved specimens, the proper thickness to be used in connection with the master curve size adjustment is the specimen nominal thickness not the net thickness.

13. Single temperature and multi-temperature MML T_0 estimation algorithms yield equivalent estimates.

14. The use of random censoring is validated.

References

1. Wallin K. The scatter in K-results. Engineering Fracture Mechanics, 1984, Vol. 19, No. 6, pp. 1085–1093.

2. Wallin, K. Optimized estimation of the Weibull distribution parameters. Espoo: Technical Research Centre of Finland, 1989. 17 p. + app. 1 p. (Research Reports 604).

3. Wallin, K. Recommendations for the application of fracture toughness data for structural integrity assessments. In: Pugh, C.E., Bass, B. R. & Keeney, J. A., Proc. of the Joint IAEA/NEA International Specialists' Meeting on Fracture Mechanics Verification by Large Scale Testing. Oak Ridge. Tennessee, 26–29 Oct. 1993. Oak Ridge: OECD, 1993. Pp. 465–494. (NUREG/CP-0131, ORNL/TM-12413 RF).

4. ASTM E1921-97. Standard test method for determination of reference temperature, T_0, for ferritic steels in the transition range. American Society for Testing and Materials, 1998, Vol. 03.01, pp. 1068–1084.

5. Wallin, K. The size effect in K_{ic} results. Engineering Fracture Mechanics, 1985, Vol. 22, No. 1, pp. 149–163.

6. Wallin, K. Fracture toughness transition curve shape for ferritic structural steels. In: Teoh, S. H. & Lee, K. H. (Eds.) Proceedings of the Joint FEFG/ICF International Conference on Fracture Engineering Materials & Structures. London: Elsevier Applied Science, 1991. Pp. 83–88.

7. Wallin, K. Irradiation damage effects on the fracture toughness transition curve shape for reactor pressure vessel steels. The International Journal of Pressure Vessels and Piping, 1993, Vol. 55, No. 1, pp. 61–79.

8. Wallin, K. Validity of small specimen fracture toughness estimates neglecting constraint corrections. In: Kirk, M. & Bakker, A. (Eds.). Constraint effects in fracture: Theory and applications. Philadelphia: American Society for Testing and Materials, 1995. 19 p. (ASTM STP 1244).

9. Wallin, K. Statistical aspects of constraint with emphasis on testing and analysis of laboratory specimens in the transition region. Constraint effects in fracture. In: Hacket, E. M., Schwalbe, K.-H. & Dodds, R. H. Jr. (Eds.). Constraint Effects in Fracture. Indianapolis, USA, 8–9 May 1991. Philadelphia: American Society for Testing and Materials, 1993. Pp. 264–288. (ASTM STP 1171).

10. Wallin, K. Macroscopic nature of brittle fracture. Journal de Physique, 1993, Vol. 3, No. IV, pp. 575–584.

11. Heerens, J. SM&T Project: Fracture toughness of steel in the ductile to brittle transition regime. Final report, Part I. GKSS Forschungszentrum, 1998. To be published.